Chitin perception in plasmodesmata identifies subcellular, context-specific immune signalling in plants

Cecilia Cheval[1], Matthew Johnston[1], Sebastian Samwald[1], Xiaokun Liu[1], Annalisa Bellandi[1], Andrew Breakspear[1], Yasuhiro Kadota[2, 4], Cyril Zipfel[2, 3] and Christine Faulkner[1]*

[1]John Innes Centre, Norwich Research Park, Colney Lane, Norwich, NR4 7UH, UK

[2] The Sainsbury Laboratory, University of East Anglia, Norwich Research Park, Colney Lane, Norwich, NR4 7UH, UK

[3] Present address: Institute of Plant and Microbial Biology, and Zürich-Basel Plant Science Centre, University of Zürich, Zollikerstrasse 107, CH-8008 Zürich, Switzerland

[4] Present address: RIKEN Centre for Sustainable Resource Science, Tsurumi-ku, Yokohama, 230-0045, Japan

*Corresponding author. Email: christine.faulkner@jic.ac.uk

Abstract

The plasma membrane (PM) that lines plasmodesmata has a distinct protein and lipid composition, underpinning specific regulation of these connections between cells. The plasmodesmal PM can integrate extracellular signals differently from the cellular PM, but it is not known how this specificity is established or how a single stimulus can trigger independent signalling cascades in neighbouring membrane domains. Here we have used the fungal elicitor chitin to investigate signal integration and responses at the plasmodesmal PM. We found that the plasmodesmal PM employs a receptor complex composed of the LysM receptors LYM2 and LYK4 which respectively change their location and interactions in response to chitin. Downstream, signalling is transmitted via a specific phosphorylation signature of an NADPH oxidase and localised callose synthesis that causes plasmodesmata closure. This demonstrates the plasmodesmal PM deploys both plasmodesmata-specific components and differential activation of PM-common components to independently integrate an immune signal.

Introduction

Plants have an interconnected cytoplasm that bridges neighbouring cells throughout. Plasma membrane-lined tubes called plasmodesmata (singular plasmodesma) cross the cell wall and establish cytoplasmic, plasma membrane (PM) and endoplasmic reticulum (ER) continuity between cells. At a single cell interface there might be thousands of plasmodesmata (Faulkner *et al.*, 2008; Danila *et al.*, 2018) and as small molecules, proteins and RNAs can pass from cell-to-cell through plasmodesmata this establishes considerable capacity for direct molecular exchange between cells and tissues. As almost all cells within plants are connected via plasmodesmata, they create an extensive conduit through which signals and resources can be distributed between cells, tissues and organs.

The functional aperture of a plasmodesma can change in response to a range of developmental and environmental signals, generating dynamic zones of connectivity and molecular exchange that underpin whole organism responses (Rinne *et al.*, 2011; Faulkner *et al.*, 2013; Lim *et al.*, 2016; Rinne, Paul and van der Schoot, 2018). Changes to plasmodesmal aperture can be executed by the synthesis and hydrolysis of the β-1,3-glucan callose in the cell wall that surrounds a plasmodesma (Rinne *et al.*, 2011; Vaten *et al.*, 2011; Cui and Lee, 2016). Enzymes responsible for callose turnover are anchored in the plasmodesmal PM and their activity is likely regulated by actors that similarly reside in the plasmodesmal PM. Indeed, several plasmodesmata-located proteins have been shown to be critical for plasmodesmal responses to a range of signals (Benitez-Alfonso *et al.*, 2013; Faulkner *et al.*, 2013; Wang *et al.*, 2013; Cui and Lee, 2016). Further, there are examples of proteins, such as the Arabidopsis CRINKLY 4 (ACR4) and CLAVATA 1 (CLV1) receptor kinases (RKs), that are resident in both the PM and the plasmodesmal PM but form plasmodesmata-specific complexes (Stahl *et al.*, 2013) suggesting that the plasmodesmal PM is a unique signalling environment.

The PM is highly organised into microdomains that are diverse in composition, function and dynamics. These microdomains regulate the organisation and activation of a variety of proteins resident within the plasma membrane. In plants and animals, this includes a variety of cell-surface proteins involved in the perception of environmental and developmental signals (Malinsky *et al.*, 2013; Ott, 2017; Gronnier *et al.*, 2018). One such class of cell surface proteins are receptors: RKs and receptor proteins (RPs) display receptor domains on the outward facing side of the PM and are critical for detecting changes in the extracellular environment and initiating downstream signalling. Plants have a large repertoire

of these PM-anchored receptors and can recognise a large range of molecular signals. Some RKs and RPs can dynamically form modular receptor complexes in PM microdomains and/or nanodomains, forming signalling hubs that execute response outputs (Lingwood and Simons, 2010; Bucherl *et al.*, 2017; Ott, 2017). For example, Medicago LysM-CONTAINING RECEPTOR-LIKE KINASE 3 (LYK3) is dynamically recruited to a PM microdomain during rhizobia infection (Liang *et al.*, 2018) and the flg22 receptor FLAGELLIN SENSING 2 (FLS2) is stabilised in nanodomains during signalling (Bucherl *et al.*, 2017). The protein and lipid composition of the plasmodesmal PM differs from other domains of the PM (Fernandez-Calvino *et al.*, 2011; Grison *et al.*, 2015; Tilsner *et al.*, 2016); the plasmodesmal PM is rich in sphingolipids (Grison *et al.*, 2015) suggesting it has similarity to PM microdomains in its lipid composition, further supporting the hypothesis that the plasmodesmal PM hosts specific signalling cascades similar to PM microdomains.

Here we have elucidated the mechanism of plasmodesmal PM specific signalling events and determined that the plasmodesmal PM functions independently of the neighbouring PM. By examining the mechanism by which cells perceive and respond to chitin, a fungal cell wall component that triggers immune responses, we have determined that signalling in the plasmodesmal PM is distinct from signalling in the PM. We found that in addition to the plasmodesmata located receptor LysM-CONTAINING GPI-ANCHORED PROTEIN 2 (LYM2) (Faulkner *et al.*, 2013), chitin responses in the plasmodesmal PM require two additional LysM RKs, LYK4 and LYK5. However, only LYK4 is detected in plasmodesmata. LYM2 can associate with LYK4 suggesting that chitin-triggered plasmodesmal responses are mediated by a chitin-activated LYM2-LYK4 complex. The dependence of plasmodesmal responses on LYK5 appears to rest on LYK5-dependent modification of LYK4 in the PM prior to chitin perception. Chitin perception by LYM2-LYK4 triggers BOTRYTIS INDUCED KINASE 1 (BIK1)-independent, calcium-dependent protein kinase mediated phosphorylation of the NADPH oxidase RESPIRATORY BURST OXIDASE HOMOLOG PROTEIN D (RBOHD) and ultimately induces callose deposition and plasmodesmata closure. These findings identify that the plasmodesmal PM integrates extracellular signals independently and specifically relative to the PM, supporting a model in which the plasmodesmal PM hosts discrete signalling cascades. Further, the independence of chitin-triggered plasmodesmal PM responses from those in the PM suggest that cell-to-cell connectivity is regulated independently of other immune responses. This work demonstrates that plasmodesmata are regulated independently of other immune responses, suggesting that there is a critical requirement for a cell to finely tune connectivity to its neighbours.

Results

Chitin-triggered plasmodesmata closure is dependent on LYK4 and LYK5

We previously identified that LYM2 is a GPI-anchored, LysM receptor protein that is resident in the plasmodesmal PM (Faulkner *et al.*, 2013). As LYM2 has no intracellular domains we reasoned that it must interact with other proteins to initiate downstream signals that result in plasmodesmal responses. Ligand perception by LysM RKs and RPs often involves multiple members of the LysM protein family: chitin perception in rice involves both the RP CHITIN ELICITOR BINDING PROTEIN (OsCEBiP) and the RK CHITIN ELICITOR RECEPTOR KINASE 1 (OsCERK1) (Kaku *et al.*, 2006; Hayafune *et al.*, 2014); peptidoglycan perception in Arabidopsis involves the RK CERK1, and RPs LYM1 and LYM3 (Willmann *et al.*, 2011); and PM chitin perception in Arabidopsis involves CERK1 (also called LYK1) and the RKs LYK4 and LYK5 (Cao *et al.*, 2014). Thus, we hypothesised that LYM2 might partner with a LysM RK for signalling. The Arabidopsis LysM RK family consists of 5 members: CERK1/LYK1, LYK2, LYK3, LYK4 and LYK5. To narrow down plasmodesmata signalling candidates we screened publicly available data sets for LYK gene expression. Comparing data sets from seedlings (GSE74955, Yamada *et al.*, 2016; GSE78735, Hillmer *et al.*, 2017) and mature leaves (eFP browser, Winter *et al.* 2007) we identified variable expression patterns for the *LYK* family members (Fig. S1). Thus, we performed RT-PCR to identify members of the family expressed in mature Arabidopsis leaves where we assay for and detect LYM2 function. Only transcripts from *CERK1*, *LYK3*, *LYK4* and *LYK5* were detected in mature leaves grown in our conditions, eliminating LYK2 from further analysis (Fig. S1). We previously showed that CERK1 is not required for chitin-triggered plasmodesmata closure (Faulkner *et al.*, 2013) and therefore we assayed for chitin-triggered plasmodesmal responses in *lyk3*, *lyk4* and *lyk5-2* mutants. Microprojectile bombardment assays, in which movement of GFP from single transformed cells within the Arabidopsis leaf epidermis is measured, demonstrated that *lyk3* mutants show a chitin-triggered reduction in the spread of GFP, indicative of plasmodesmata closure (Fig. 1) comparable to the wild-type (Col-0) response. By contrast, *lyk4* and *lyk5-2* mutants show no change in GFP spread following chitin treatment identifying that these mutants cannot close their plasmodesmata in response to chitin similar to *lym2* mutant plants. Thus, LYK4 and LYK5 are required for chitin-triggered plasmodesmata closure.

LYM2-dependent chitin-signalling induces callose deposition at plasmodesmata

Callose is a β-1,3-glucan polymer deposited at plasmodesmata during stages of development and in response to a range of stresses inducing functional plamodesmal closure (Wang *et al.*, 2013; Cui and Lee, 2016; Xu *et al.*, 2017). It is established that reactive oxygen species (ROS) induce plasmodesmal callose deposition and recently we showed that callose is deposited at plasmodesmata in response to flg22 (Xu *et al.*, 2017). Therefore, we examined callose deposition at plasmodesmata in response to chitin in Arabidopsis to determine if this is common to pathogen-triggered plasmodesmata closure. We quantified aniline blue-stained plasmodesmata-located callose deposits in chitin-treated and mock-treated leaf tissue of WT plants and, as for flg22, plasmodesmata-located aniline blue fluorescence increased significantly within one hour of chitin treatment (Fig. 1B, C). This indicates that callose deposition at plasmodesmata in response to chitin is an early immune response, likely triggered within the timeframe of other rapid PAMP-triggered responses such as the ROS burst and MAPK activation. Aniline blue staining of *lym2-1*, *lyk4* and *lyk5-2* mutant leaves in the presence of chitin showed that each mutant is unable to deposit callose at plasmodesmata in response to chitin, confirming that the chitin-triggered reduction in GFP movement through plamsodesmata is caused by callose deposition. *lym2-1* mutant leaves showed a reduction in plasmodesmal callose in response to chitin. Like Col-0, *cerk1-2* mutants show an increase in plasmodesmal callose deposition in response to chitin, consistent with the chitin-triggered reduction in GFP movement through plasmodesmata by the bombardment assay.

LYK4 is present in plasmodesmata

Having identified that LYK4 and LYK5 are required for chitin-triggered plasmodesmata closure we examined their subcellular localisation to determine if they accumulate at plasmodesmata like LYM2. We generated translational fusions of LYK4 and LYK5 to RFP. Both LYK4 and LYK5 localised to the PM in the absence and presence of chitin, with no enrichment in plasmodesmata evident (Fig. S2). Plasmodesmata are smaller than the limits of resolution of a confocal microscope and if there is no enrichment of protein at the plasmodesmata relative to the PM it is difficult to conclude absolutely whether the protein is present or absent from plasmodesmata. Thus, we performed subcellular fractionation of plasmodesmata and protein extraction to determine the presence or absence of LYK4 and LYK5 in plasmodesmal fractions (Fig. 2A). For this we expressed LYK4-HA, LYK5-HA or the plasmodesmal protein PDLP5-HA (Lee *et al.*, 2011) in *N. benthamiana*

tissue and purified plasmodesmata. We could detect PDLP5-HA and LYK4-HA, in purified plasmodesmal extracts, but not LYK5-HA, identifying that only LYK4 co-locates with LYM2 at plasmodesmata. This suggests that despite the genetic dependence of chitin-triggered plasmodesmata closure on *LYM2*, *LYK4* and *LYK5*, these three receptors do not necessarily act co-operatively within plasmodesmata.

LYM2 associates with LYK4

The presence of LYM2 and LYK4 in the plasmodesmal PM suggests that they may form a functional complex that triggers plasmodesmal responses. To test this hypothesis, we determined if LYM2 associates with LYK4 by targeted co-immunoprecipitation (co-IP) assays. We co-expressed Citrine-LYM2 with LYK4-HA in *N. benthamiana* and immunoprecipitated Citrine-LYM2 from membrane fractions with anti-GFP beads (Fig. 2B). LYK4-HA was co-immunoprecipitated with LYM2 from both water and chitin treated tissue suggesting that LYM2 associates with LYK4 in a chitin independent manner. The negative control BRI1-RFP did not co-immunoprecipitate with Citrine-LYM2 (Fig. S3A).

Given that LYM2 and LYK4 are present in plasmodesmata we thought that these two proteins could directly execute plasmodesmal PM chitin signalling. However, LYK5 is also required for chitin-triggered plasmodesmata closure and thus, we tested the dependence of the interaction between LYM2 and LYK4 on LYK5. For this we transformed Arabidopsis *lyk5-2* protoplasts with Citrine-LYM2 and LYK4-RFP (Fig. 2C) and performed targeted co-IPs. We observed that LYK4-RFP immunoprecipitated with Citrine-LYM2 in a chitin-independent manner from both Col-0 and *lyk5-2* protoplasts. While this clearly demonstrates that the interaction between LYM2 and LYK4 is LYK5 independent, these assays also identified that LYK4-RFP appears approximately 10 kDa smaller on SDS-PAGE gels when extracted from *lyk5-2* protoplasts, suggesting that LYK4 is modified in a LYK5 dependent manner. Further, following chitin treatment the dominant LYK4-RFP band detected in *lyk5-2* protoplasts appears approximately 30kDa smaller than the dominant band in the WT protoplasts suggesting that the 'non-modified' variant of LYK4-RFP in the *lyk5-2* mutant is subject to degradative processing in response to chitin. Given the genetic dependence of chitin-triggered plasmodesmata closure on *LYK5*, these observations suggest that modification of LYK4 mediated by LYK5 is essential for its plasmodesmata-related signalling function.

194

195 *LYK4 and LYK5 associate in the PM*

196 The observation that LYK5 is required for both chitin-triggered plasmodesmata
197 closure and modification of LYK4, but is not located at plasmodesmata, suggests a model in
198 which LYK5 plays a spatio-temporally distinct role in chitin-triggered plasmodesmata
199 closure. To further investigate we explored the possibility that LYK5 associates with and
200 modifies LYK4 in the PM, upstream of LYK4 activity at plasmodesmata. Pull-downs of
201 LYK4-GFP from membrane fractions of *N. benthamiana* tissue expressing both LYK4-GFP
202 and LYK5-RFP showed that LYK5-RFP co-immunoprecipitates with LYK4-GFP (Fig. 3A).
203 The negative control BRI1-RFP did not co-immunoprecipitate with LYK4-GFP (Fig. S3B).
204 This suggests that LYK4 and LYK5 associate in the PM.

205 We further explored the dynamics of this interaction with FLIM-FRET analysis (Fig.
206 3B). The fluorescence lifetime (average amplitude, T_{Av}) of PM-localised LYK4-GFP was
207 significantly reduced in the presence of LYK5-RFP, indicating an increase in FRET as
208 expected for interacting proteins. Chitin-treatment decreased the degree of FRET observed
209 between LYK4-GFP and LYK5-RFP suggesting that chitin weakened the interaction between
210 LYK4 and LYK5 by either complex dissociation or a change in conformation.

211 We also used FRET-FLIM to investigate the localisation of a LYK4-LYK5 complex
212 and compare the PM with the plasmodesmal PM (Fig. 3C). For this we marked
213 plasmodesmata by co-expression of LYK4-GFP and LYK5-RFP with Citrine-LYM2. When
214 we compared T_{Av} of LYK4-GFP in regions of interest (ROIs) within the PM and ROIs at
215 plasmodesmata we observed that in the PM T_{Av} was significantly reduced by the presence of
216 LYK5-RFP as expected, but that in plasmodesmata it was not reduced. This supports our
217 finding that LYK5 is not present in the plasmodesmal PM, and the hypothesis that LYK5 is
218 critical for LYK4 function upstream of plasmodesmal signalling.

219

220 *LYM2, LYK4 and LYK5 are dynamic in response to chitin*

221 It has been shown that LYK5 undergoes re-localisation in the form of endocytosis in
222 response chitin (Erwig *et al.*, 2017) and so we explored possible dynamics of LYM2 in
223 response to chitin. Live-cell imaging of Citrine-LYM2 in *N. benthamiana* leaves suggested
224 that Citrine-LYM2 fluorescence at plasmodesmata increased in response to chitin treatment
225 (Fig. 4A); i.e. Citrine-LYM2 at plasmodesmata appeared to get brighter relative to PM

fluorescence following chitin treatment. We quantified this response by measuring the plasmodesmal index (PD index) of fluorescence (plasmodesmata:PM fluorescence intensity (Perraki *et al.*, 2018) for LYM2 in the absence and presence of chitin (Fig. 4B). The mean PD index of Citrine-LYM2 in mock treated samples was 1.7 but following 30 min chitin treatment increased to 2.5, indicating a significant increase in fluorescence intensity at plasmodesmata in response to chitin. Fluorescence anisotropy measurements of Citrine-LYM2 in chitin-treated tissue identified lower anisotropy in the plasmodesmata relative to the PM indicating there is more homo-FRET occurring at plasmodesmata (Fig 4C). The observation that anisotropy (*r*) of Citrine-LYM2 is lower in the PM relative to freely rotating cytosolic GFP suggests that homo-FRET occurs in the PM, *i.e.* that LYM2 can interact with itself in the PM. That *r* is further reduced in plasmodesmata suggests that Citrine-LYM2 forms a higher order complex or signalling platform in the plasmodesmal PM.

We did not observe any robust change in the distribution of fluorescence of either LYK4-RFP or LYK5-RFP in response to chitin by live-imaging in *N. benthamiana* leaves (Fig. S2). However, FRET-FLIM data suggests that LYK4 and LYK5 dissociate in response to chitin, which could lead to increased lateral mobility of LYK4 and LYK5. To test this, we performed FRAP analysis of LYK4-RFP and LYK5-RFP in mock and chitin-treated tissue (Fig. 4D). Following chitin treatment, the mobile fraction of both LYK4 and LYK5 within the PM increased. Citrine-LYM2 also exhibited a marginal increase in the mobile fraction of molecules in response to chitin, but only at plasmodesmata. This elevation in the proportion of the mobile fraction of each receptor in response to chitin suggest dynamic behaviour of these receptors that changes their interactions and/or the membrane domains in which they reside.

LYM2-dependent chitin-triggered plasmodesmata closure engages unique calcium/ROS regulatory modules

Reactive oxygen species (ROS) are produced in immune responses and can induce plasmodesmata closure (Torres, Dangl and Jones, 2002; Cui and Lee, 2016). Thus, we hypothesized that ROS play a role in the regulation of plasmodesmata closure in response to chitin, downstream of LYM2-LYK4 activity. We firstly verified that H_2O_2 -induced plasmodesmata closure can be detected by the bombardment method and observed a reduction of GFP movement from cell-to-cell in WT plants after H_2O_2 treatment (Fig. S4). In

this assay, *lym2-1* mutants were able to close their plasmdesmata in response to H_2O_2 demonstrating that any role for ROS signalling in chitin-triggered plasmodesmata closure occurs independently, or downstream of LYM2 activity. We also further established that transient expression of LYM2, LYK4 and LYK5 enhanced ROS production in *N. benthamiana* leaf discs following chitin treatment, suggesting that each of these LysM proteins can mediate ROS signalling.

The rapid production of ROS in response to chitin is associated with the NADPH oxidase RBOHD (Kadota *et al.*, 2014) and so we tested whether RBOHD is required for chitin-triggered plasmodesmata closure. Bombardment assays showed that the *rbohd* mutant is not able to close its plasmodesmata in response to chitin treatment (Fig. 5A). This was supported by quantitative analysis of plasmodesmal callose that showed that *rbohd* mutants did not deposit callose at plasmodesmata in response to chitin (Fig. S5). Thus, ROS produced by RBOHD are a critical component of the chitin-triggered signalling cascade that induces plasmodesmata closure.

In Arabidopsis, RBOHD is regulated by phosphorylation by protein kinases (Dubiella *et al.*, 2013; Kadota *et al.*, 2014, 2018; Li *et al.*, 2014). It has been shown that the receptor-like cytoplasmic kinase (RLCK) BIK1 and calcium dependent protein kinases (CPKs) both phosphorylate RBOHD in response to chitin: BIK1 phosphorylates Ser39, Ser339, Ser343 and Ser347, while CPKs phosphorylate Ser133, Ser148, Ser163 and Ser347 (Dubiella *et al.*, 2013; Kadota *et al.*, 2014). To test dependence of plasmodesmal responses on BIK1, we assayed *bik1* mutant plants for chitin-triggered plasmodesmata closure and observed that *bik1* mutants exhibited a wild-type response to chitin. Thus, BIK1 does not function in this process (Fig. 5A). Given the large number of members in the RLCK and CPK families that function in immune responses we focused our attention on the contribution of phosphorylated residues of RBOHD to chitin-triggered plasmodesmal responses. For this we tested a range of phospho-null mutant variants (mutation of serine to alanine) of RBOHD in the *rbohd* mutant background: $RBOHD_{S39A/S339A/S343A}$, $RBOHD_{S343A/S347A}$, $RBOHD_{S133A}$, and $RBOHD_{S163A}$ (Fig. 5A). Consistent with our results for the *bik1* mutant, $RBOHD_{S39A/S339A/S343A}$, in which serines phosphorylated by BIK1 are mutated, showed a wild-type response and can close their plasmodesmata in response to chitin. Examining variants in which mutated phosphosites are targeted by CPKs, $RBOHD_{S343A/S347A}$ and $RBOHD_{S133A}$ were unable to close their plasmodesmata in response to chitin while $RBOHD_{S163A}$ showed a wild-type response, identifying that phosphorylation of S347 and S133 are required for chitin-triggered plasmodesmata closure. Thus, unlike the CERK1-mediated ROS burst at the PM (Miya *et al.*,

2007; Rao *et al.*, 2018), chitin-triggered plasmodesmata closure is independent of BIK1 and instead dependent on CPK mediated phosphorylation of RBOHD.

Among the CPKs, CPK4, 5, 6 and 11 have been described to be involved in the regulation of RBOHD-dependent ROS burst, and CPK6 has been shown to phosphorylate both Ser133 and S347 (Kadota *et al.*, 2014). Therefore, we tested the involvement of CPK6 in chitin-triggered plasmodesmata closure. Bombardment assays showed that two independent *cpk6* mutants, *cpk6-1* and *cpk6-2*, were unable to close their plasmodesmata in response to chitin (Fig. 5A) confirming CPK6 functions in plasmodesmal signalling.

LYM2 is a GPI anchored protein and therefore unlikely to directly interact with intracellular CPKs. Having shown previously that LYM2 associates with LYK4 (Fig 2), we investigated the interaction between CPK6 and LYK4. We generated a GFP-tagged translational fusion of CPK6 (CPK6-GFP) that we transiently expressed in *N. benthamiana* leaf tissue with LYK4-HA. Co-IP experiments show that CPK6-GFP and LYK4-HA associate (Fig 5B). These data suggest that a LYM2-LYK4 complex recruits CPK6 for phosphorylation of RBOHD and thereby executes plasmodesmal signalling.

Discussion

The innate immune system depends on the perception of pathogen molecules by extracellular and intracellular receptors. Here, we have characterised how a plant cell can perceive and initiate immune responses to a single ligand in different domains of the PM. Our data has identified that while fungal chitin is perceived and triggers signalling via a CERK1-dependent cascade in the PM, in the plasmodesmal PM chitin triggers a LYM2/LYK4-dependent cascade to produce a specific, localised response. Thus, for chitin signalling in plant cells both receptors and signalling cascades can show specificity to a given subcellular context.

Subcellular specificity in ligand perception by receptors and signalling have both been documented in animal cells. It is known that the same ligand can be perceived by different receptors in different subcellular compartments, allowing detection of a ligand in different cellular locations, e.g. the flg22 peptide can be perceived extracellularly by the membrane anchored Toll-Like Receptor 5 (TLR5) (Hayashi *et al.*, 2001) and in the cytosol by the soluble NLR Family CARD Domain Containing 4 (NLRC4) (Kofoed and Vance, 2011; Zhao *et al.*, 2011). Alternatively, subcellular specificity can be conveyed at the response level, e.g. the lipopolysaccharide (LPS) receptor TLR4 triggers signalling from the PM but is also

endocytosed and subsequently initiates a secondary signalling cascade from endosomes (Płóciennikowska *et al.*, 2015). Our findings here show that plant cells can combine both receptor and signalling specialisation to fully integrate the perception of a signal into an immune response. Further, specialisation and independence of signalling at the plasmodesmal PM suggests that cell-to-cell connectivity must be regulated independently of other immune outputs, raising questions regarding whether there is a critical requirement for cells to balance communication and exchange with the protective mechanism imposed by isolation.

Our investigation in to the mechanisms by which chitin signalling is executed at the plasmodesmal PM identified that the plasmodesmata-resident GPI-anchored protein LYM2 accumulates at plasmodesmata in response to chitin. LYM2 also exhibits greater homo-FRET in the plasmodesmal PM than in the PM suggesting it oligomerises or clusters to form a signalling platform. It is well established that many forms of immune signalling occur via the formation of supramolecular complexes such as signalosomes and inflammasomes that involve the oligomerisation of cytosolic NLR receptors and downstream signalling components. Membrane anchored receptors also form multi-component signalling complexes (Mueller and Nickel, 2012; Stegmann *et al.*, 2017; Ren *et al.*, 2019) and in some cases higher order clusters (Scott *et al.*, 2008; Pan *et al.*, 2019) for signalling. The CYSTEINE-RICH RECEPTOR-LIKE KINASE2 (CRK2) was recently shown to accumulate at the plasmodesmal PM in response to salt stress (Hunter *et al.*, 2019) suggesting the possibility that the plasmodesmal PM commonly executes signalling via transient recruitment and concentration of machinery.

We found that in addition to LYM2, the RK LYK4 is also critical for plasmodesmal PM chitin signalling. LYK4 associates with LYM2 and is detected in plasmodesmata but does not accumulate at plasmodesmata in response to chitin. LYK4 associates with the RK LYK5 in the PM but in response to chitin treatment we observed that the mobile fraction of LYK4 increased and the association between LYK4 and LYK5 in the PM decreased. When membrane proteins change their associations, they frequently exhibit a change in their biophysical properties and/or behaviour and therefore our data suggests that chitin triggers dissociation between these two RKs and releases a pool of LYK4 for signalling at plasmodesmata. It has been reported that the mobility of receptors both increases (Wang *et al.*, 2015) and decreases (Bucherl *et al.*, 2017) in response to ligand binding, but given that signalling complexes are larger multi-component structures, it is likely that activated receptors in complexes are less mobile. Our observations of an increased mobile fraction in

response to the presence of chitin might result from the complex dynamics and changes in association that are evident for the LysM receptor family and represent the disassociated fraction of the RK pool. It might also be that LysM receptors and their signalling complexes behave differently from the LRR receptors that have been the focus of previous studies.

In addition to LYM2 and LYK4 we identified that LYK5 is a critical component of chitin-triggered plasmodesmal responses. However, LYK5 was not detected in purified plasmodesmata. This suggested to us that the dependence of chitin-triggered plasmodesmata closure on LYK5 is due to activity and association with LYK4 in the PM, upstream of plasmodesmal signalling responses. Targeted co-IP of LYM2 and LYK4 from *lyk5-2* protoplasts identified that LYK4 was smaller in the absence of LYK5 and undergoes enhanced degradative processing in response to chitin. It is known that LysM receptors are subject to ectodomain cleavage (Petutschnig *et al.*, 2014), which might explain the chitin-triggered degradation of LYK4. However, the smaller form of LYK4 detected in *lyk5-2* protoplasts is more consistent with a post-translational modification such as mono-ubiquitination or sumoylation. Indeed, LYK5 has been shown to interact with the E3 ubiquitin ligase PLANT U-BOX13 (Liao *et al.*, 2017) suggesting ubiquitination is a likely candidate modification. Thus, we propose that LYK5 is required for post-translational modification of LYK4 so that it can execute plasmodesmal responses.

LYK4 is predicted to be an inactive kinase (Wan *et al.*, 2012), suggesting that it needs further interacting partners to mediate signalling. Here, we have shown LYK4 can associate with CPK6, which is known to phosphorylate Ser133 and Ser347 of RBOHD (Kadota *et al.*, 2014) and is critical for chitin-triggered plasmodesmata closure. Thus, CPK6 could transmit a signal from LYK4 to RBOHD in the plasmodesmal PM. In this scenario, LYK4 has characteristics of a scaffold protein that modulates signalling complex formation: LYK4 bridges the apoplastic plasmodesmal-specificity defined by LYM2 with an intracellular signalling kinase. This has some similarity to the activity described recently for the malectin-like receptor kinase FERONIA (FER) (Stegmann *et al.*, 2017) and the N-myristoylated protein BRASSINOSTEROID SIGNALING KINASE 3 (BSK3) (Ren *et al.*, 2019) in the formation of receptor signalling complexes for EF-Tu and flg22, and brassinosteroids respectively.

Current models for phosphorylation and activation of RBOHD have suggested that RLCKs and CPKs are involved in a two-step regulation of RBOHD activity in which RLCKs prime RBOHD for activation by CPK phosphorylation (Kadota *et al.*, 2014). This idea allows for finely tuned control of the production of ROS. In our study, chitin-triggered

plasmodesmata closure is independent of BIK1, one of the RLCK family members required for the CERK1 associated chitin-triggered ROS burst (Rao *et al.*, 2018). Chitin-triggered plasmodesmata closure is unlikely to depend on other RLCKs as the response is also independent of phosphorylation of Ser39, Ser339 and Ser343 which are targeted by the RLCK BIK1 and essential for the CERK1 associated chitin-triggered ROS burst (Kadota *et al.*, 2014). Thus, our data suggests that for chitin-triggered plasmodesmata closure, RBOHD activity might be controlled by different regulatory modules. It is unclear what information specific activation of RBOHD conveys in independent signalling pathways to a single ligand.

We observed that chitin-triggered plasmodesmata closure is dependent on both CPK-targeted phosphosites within RBOHD, and CPK6. However, not all CPK targeted phosphosites of RBOHD we tested were critical for plasmodesmal responses. Mutation of Ser163 did not abolish chitin-triggered plasmodesmata closure while mutations in Ser133 and Ser347 did, implying there is response-associated specificity within CPK-mediated phosphorylation of RBOHD. A possible explanation lies in CPK phosphorylation motifs (Kadota *et al.*, 2014): Ser133 and Ser347 are categorised as motif 1 sites ([B-B-X-B]-φ-X-X-X-X-S/T-X-B) while Ser163 is categorised as a motif 2 site (φ-X-B-X-X-S-X-X-X-φ) linking chitin-triggered plasmodesmata closure to motif 1 sites. The significance of these motifs and their relevance to plasmodesmal signalling is unknown; they may correlate to specific CPKs, or to an independent mechanism for tuning RBOHD activity.

Combining all the measurements and observations we have made in this study, we propose a model for plasmodesmal PM specific signal integration during chitin immune responses (Fig. 6). We suggest that LYK4 and LYK5 constitutively interact at the PM and that this mediates function-critical modification of LYK4. Chitin perception triggers dissociation of the LYK4-LYK5 complex, allowing for an increased interaction between LYK4 and LYM2, and LYM2 accumulation at plasmodesmata. At the plasmodesmal PM, LYM2 establishes a signalling platform that recruits LYK4, and by association CPK6, to this membrane microdomain. CPK6 phosphorylates RBOHD to produce ROS and induce localised callose synthesis and plasmodesmata closure within an hour of the initial perception of chitin.

This model is distinct from that for chitin perception in the PM in which a CERK1-LYK5 complex forms in response to chitin and triggers BIK1-dependent phosphorylation of RBOHD. Both the plasmodesmal PM and PM chitin-triggered signalling cascades activate RBOHD, but our analyses identified that CERK1 and LYM2 signalling function independently (Faulkner *et al.*, 2013). It is significant that while both chitin responses

activate RBOHD there is no evidence of cross-talk between the ROS produced by CERK1 and LYM2. This independence suggests either that ROS signalling is highly localised. Alternatively, it is possible that the apoplastic environment surrounding the plasmodesmata insulates the plasmodesmal PM from external signals, but the observation that exogenously applied hydrogen peroxide can induce plasmodesmal responses (Fig. S5; Cui and Lee, 2016) suggests this is unlikely to fully explain the signalling localisation.

We have demonstrated that the plasmodesmal PM integrates signals independently of the PM and that plant cells are thus capable of exploiting receptor and signalling specificity to mediate localised and specialised responses. In the context of immune responses, this identifies that cells regulate cell-to-cell connectivity independently of other immune outputs. This work establishes that cell-to-cell connectivity and molecular exchange is a key component of how plant tissues respond to pathogen signals. Given that plasmodesmata are regulated in response to a range of abiotic and developmental signals it seems likely that the ability of a cell to independently regulate its plasmodesmata occurs in a variety of contexts and is a fundamental component of how tissues and organs respond as multicellular entities.

Material and methods

Plant materials

Arabidopsis plants were grown on soil in short days conditions with 10h light at 22 °C. *N. benthamiana* plants were grown on soil with 16h light at 23 °C. Arabidopsis Columbia-0 (Col-0) was used as wild-type plants. The mutant lines used in this study are: *rbohd* (Torres, Dangl and Jones, 2002), *lym2-1* (SAIL_343_B03, (Faulkner *et al.*, 2013)), *cerk1-2-* (GABI_096F09, (Miya *et al.*, 2007)), *lyk3* (SALK_140374 (Wan *et al.*, 2012)), *lyk4* (WiscDsLox297300_01C (Wan *et al.*, 2012)), *lyk5-2* (SALK_131911.31.20.x (Cao *et al.*, 2014)), *bik1* (Salk_005291C (Veronese *et al.*, 2006)), *cpk6-1* (SALK_093308) and *cpk6-2* (SALK_033392) (Mori *et al.*, 2006). RBOHD variants $RBOHD_{S339A/S343A}$ and $RBOHD_{S39A/S339A/S343A}$ are mutant variants of RBOHD transformed in to the *rbohd* mutant background as described (Kadota *et al.*, 2014). The RBOHD variants $RBOHD_{S133A}$ and $RBOHD_{S163A}$ were generated by complementation of the Arabidopsis *rbohd* mutant with constructs harbouring site specific mutations.

DNA Constructs

Citrine-LYM2 is as previously described (Faulkner *et al.*, 2013). LYK4 and LYK5 coding sequences were PCR amplified from Col-0 cDNA and cloned into pDONR by Gateway BP reactions (Invitrogen). Entry Clones carrying LYK4 and LYK5 were verified by sequencing. To generate Cauliflower Mosaic Virus (CaMV) 35S promoter-driven LYK4 and LYK5 constructs C-terminally-tagged with GFP, RFP, HA or myc, pENTR clones were recombined by the Gateway LR reaction with pB7FWG2.0, pB7RWG2.0, pGWB14 and pGWB17 respectively. CPK6 was PCR cloned from Col-0 cDNA using gene-specific primers with Golden Gate compatible extensions (BpiI recognition sequences and fusion sites) and cloned into the universal acceptor plasmid pUAP1 by digestion/ligation using BpI1. Clones were validated by sequencing. Level 1 binary constructs were assembled in the pICH47751 vector with the following modules by digestion/ligation using BsaI: pUAP1 carrying CPK6; pICH51277 carrying CaMV 35S, pICSL50008 carrying GFP for C-terminal fusion, pICH41414 carrying CaMV 35S terminator. The BRI1-RFP fusion is as described (Bucherl *et al.*, 2017). For generation of $RBOHD_{S133A}$ and $RBOHD_{S163A}$ we used site-directed mutagenesis: DNA fragments were amplified by PCR using primers harbouring mutation from pBIN19g.pRbohD:3xFLAG-gRBOHD (Kadota *et al.*, 2014) and the mutated fragments were cloned between EcoRI and BamHI sites of pBin19g vector by using In-fusion enzyme.

Transient expression in *Nicotiana benthamiana*

Agrobacterium tumefaciens GV3101 carrying the desired construct was cultured overnight and resuspended in MMA buffer containing 0.01M 2-(N-morpholino)ethanesulfonic acid (MES) pH 5.6, 0.01M $MgCl_2$, 0.01M acetosyringone. Each *Agrobacterium* strain carrying the desired construct was mixed with an *Agrobacterium* strain carrying the P19 silencing suppressor. Each strain was adjusted to a final optical density of 0.2 at 600 nm and syringe-infiltrated into leaves of 4-week-old *Nicotiana benthamiana* plants. Material for experiments was harvested two days post-infiltration.

Semi-quantitative RT-PCR analysis

RNA was extracted from leaves of 5-week-old Arabidopsis plants using RNeasy Mini extraction kit (Qiagen) and treated with Turbo DNA-free kit (Ambion) before cDNA synthesis using Reverse Transcriptase (Promega) according to the manufacturer's instructions. Semi-quantitative RT-PCR was performed on the cDNA samples with primers listed in Table S2.

Microprojectile bombardment assays

Microprojectile bombardment assays were performed as described (Faulkner *et al.*, 2013). 5- to 6-week-old expanded leaves of *Arabidopsis* plants were bombarded with 1nm gold particles (BioRad) coated with pB7WG2.0-GFP and pB7WG2.0-RFP_{ER}, using a Biolostic PDS-1000/He particle delivery system (BioRad). The gold particles were prepared by precipitating 5 µg of each DNA plasmid construct on to the gold particles with 625mM $CaCl_2$ (Sigma) and 10mM spermidine (Sigma). Bombarded leaves were infiltrated with 500 µg/mL chitin (mixture of chitin oligosaccharides, NaCoSy) or water 2 hours post bombardment. Bombardment sites were assessed 16 hours after bombardment by confocal (Leica SP5 or SP8) or epifluorescence microscopy (Leica DM6000) with a 25× water dipping objective (HCX IRAPO 25.0× 0.95 water). The number of cells showing GFP was counted for each bombardment site (marked by RFP_{ER}). For each treatment, data were collected from at least 3 independent experiments, each of which consisted of leaves from at least three individual plants. The normality of each data set was assessed by a Shapiro-Wilk test. When normally distributed a Student's t-test was applied and when the data was not normally distributed a non-parametric Mann-Whitney U test was used. Statistical significance was concluded when p-value was less than 0.05. Sample-specific details are listed in the figure legends.

Protoplast preparation and transfection

Protoplasts were extracted and transfected as described previously (Yoo, Cho and Sheen, 2007). True leaves from 4-5-week-old Arabidopsis plants were cut in 1mm leaf strips using a razor blade. Leaf strips were immediately submerged into an enzyme solution containing 20mM MES (Sigma) pH 5.7, 1.5% (w/v) cellulase R10 (Yakult Pharmaceuticals, Japan), 0.4% (w/v) macerozyme R10 (Yakult Pharmaceuticals, Japan), 0.4M mannitol, 20mM KCl, 10mM $CaCl_2$ and 0.1% bovine serum albumin (BSA). The enzyme solution was warmed to at 55 ^{o}C for 10min and filtered with 0.45µm syringe filter before use. Leaf strips were vacuum-infiltrated for 30 minutes in the dark and left at room temperature in the dark for 3 hours. The protoplasts in solution were then diluted with an equal volume of W5 solution containing 2mM MES pH 5.7, 154mM NaCl, 125mM $CaCl_2$, 5mM KCl and filtered with a 75µm nylon mesh. Protoplasts were pelleted in a 30ml round-bottom Oak Ridge centrifuge tube at 150*g*, for 1min and re-suspended at $2x10^5$ ml^{-1} in W5 solution (the number of protoplasts was counted using a haemocytometer). Protoplasts were kept on ice for 30 minutes, pelleted at 150*g* and re-suspended at $2x10^5$ ml^{-1} in MMG solution containing 4mM MES pH 5.7, 0.4M mannitol and 15mM $MgCl_2$, at room temperature before DNA/PEG/Calcium transfection. For transfection, 10µg of plasmid DNA was mixed gently with 100µl of protoplasts and 110µl PEG/Calcium solution containing 20% (w/v) PEG4000, 0.2M mannitol and 100mM $CaCl_2$. The transfection mixture was incubated at room temperature for 5 minutes, diluted with W5 solution and centrifuged at 100*g* for 2min. Protoplasts were then re-suspended in WI solution containing 4mM MES pH 5.7, 0.5M mannitol and 20mM KCl and incubated at room temperature for about 16 hours. Transfected protoplasts in WI were centrifuged at 100g for 2min, the supernatant was removed, and the pellet was frozen on dry ice before being stored at -70 ^{o}C for further analyses.

Microscopy

Confocal microscopy was performed on a Leica SP5, Leica SP8, or ZEISS LSM800 with a 25× water-dipping lens (HCX IRAPO 25.0 × 0.95 water), a 40× oil immersion lens (HCX PLAPO CS 40.0× 1.25 OIL), a 63× oil immersion lens (Plan-APOCHROMAT 63×/1.4 oil) or a 63×/1.2 water immersion objective lens (C-APOCHROMAT 63×/1.2 water). Citrine was excited with a 488 nm or 514 nm argon laser and collected at 525–560 nm. mRFP and mCherry were excited with a 561 nm DPSS laser and collected at 600-640 nm, GFP was

539 excited with a 488 nm argon laser and collected at 505-530 nm, aniline blue was excited with
540 a 405 nm UV laser and collected at 430-550 nm.

541 **Plasmodesmal callose staining and quantification**

542 Plasmodesmal callose staining and quantification was performed as described (Xu *et al.*,
543 2017). The 8th leaf of 5-6-week-old Arabidopsis plants was infiltrated with water or chitin.
544 One hour after treatment, the leaf tissue was infiltrated with 0.01% aniline blue in PBS buffer
545 (pH 7.4). Three areas were cut from one leaf and three different sites were imaged from each
546 area. Callose deposits were imaged from the abaxial side of the leaf using a 63× oil
547 immersion lens (Plan-APOCHROMAT 63×/1.4 oil) with a Leica SP5 confocal microscope.
548 Aniline blue was excited with a 405 nm UV laser and collected at 430-550 nm. This was
549 replicated for 5-12 leaves per genotype and treatment. Aniline blue stained plasmodesmal
550 callose was quantified using automated image analysis pipeline "find plasmodesmata" written
551 in Python (Xu *et al.*, 2017) (https://github.com/JIC-CSB/find-plasmodesmata). Three-
552 dimensional segmentation was carried out by initially thresholding the input image
553 (experimentally adjusted: default min 8000, max 15000). The resulting binary image was
554 then segmented by connected component analysis. Post segmentation filtering was based on
555 the number of voxels in each connected component. Objects <2 voxels (noise) and objects
556 >100 voxels (callose accumulated in stomata) were removed. All annotated images were
557 sanity checked prior to inclusion of data in the final set. The normality of each data set was
558 assessed by a Shapiro-Wilk test. When normally distributed a Student's t-test was applied and
559 when the data was not normally distributed a non-parametric Mann-Whitney U test was used.
560 Statistical significance was concluded when p-value was less than 0.05. Sample-specific
561 details are listed in the figure legends.

562 **PD index (plasmodesmata/PM fluorescence intensity ratio)**

563 Leaves of *N. benthamiana* transiently expressing the constructs of interest were observed 30
564 min after infiltration with chitin (500 µg/mL) or water (mock conditions) for PD index
565 determination. The abaxial side of the leaf samples was imaged using a 63×/1.2 water
566 immersion objective lens (C-APOCHROMAT 63×/1.2 water) with either a Leica SP8 or
567 Zeiss LSM800 confocal microscope. PD index was determined by measuring the intensity
568 values of Citrine-LYM2 at plasmodesmata and in two surrounding PM regions with ImageJ.
569 PD index values were averaged for each image and 31 images for mock and chitin treatments
570 were analysed by a Student's t-test.

571 **Fluorescence Anisotropy**

572 Leaves of *N. benthamiana* transiently expressing Citrine-LYM2 and cytosolic GFP were
573 imaged with a Leica SP8 confocal microscope. Citrine was excited with a pulsed white light
574 laser (488 nm) and emitted light was separated in to parallel and perpendicular polarizations
575 and detected by external SPADs with 500-550 nm filters. A series of 20 frames were merged
576 and analysed using PicoQuant SymPhoTime 64. Anisoptropy (*r*) was calculated by

577 $$r = \frac{I_{\parallel} - GI_{\perp}}{(2 - 3L_1)I_{\perp} + (1 - 3L_2)I_{\parallel}}$$

578 where G=0.481, L_1=0.013 and L_2=0.037. ROIs were defined that correlated to
579 plasmodesmata and the PM for Citrine-LYM2 images or the cytosol for GFP images.

580 **FRET-FLIM analysis**

581 Leaves of *N. benthamiana* transiently expressing the constructs of interest were used 30 min
582 after infiltration with chitin (500 µg/mL) or water (mock conditions) for FRET-FLIM. The
583 abaxial side of the leaf samples was imaged using a 63x/1.2 water immersion objective lens
584 (Leica C-APOCHROMAT 63×/1.2 water). FLIM experiments were performed using a Leica
585 TCS SP8X confocal microscope equipped with TCSPC (time correlated single photon
586 counting) electronics (PicoHarp 300), photon sensitive detectors (HyD SMD detector), a
587 pulsed laser (white light laser, WLL) with a range from 470 to 670nm. The WLL at 488 nm
588 was used to excite GFP at 488nm. Laser power was kept low (0.5-3%) to avoid any bleaching
589 of the samples. GFP emission was collected between 509-530nm. The repetition rate was set
590 up to 40Mhz. Additional 488nm and 561nm notch filters were used to reduce interference
591 reflected light. The instrument response function (IRF) was measured using erythrosine B as
592 described (Stahl *et al.*, 2013). The FLIM data sets were recorded using the Leica LASX
593 FLIM wizard linked to the PicoQuant SymPhoTime 64 software. The FLIM data sets were
594 acquired by scanning each image until a suitable number of photon counts per pixel
595 (minimum 1000) was reached. For the acquisition, the image size was set to 250 × 50 pixels
596 with a speed of 50Hz, allowing a pixel dwell time of 19µs. The laser power was adjusted to
597 reach a maximum count of 2000 kcounts per second. Each acquisition was stopped after 40
598 frames. Data were analysed by obtaining excited-state lifetime values of a region of interest
599 (plasma membrane or plasmodesmata). Calculations were performed using the PicoQuant
600 SymPhoTime 64 software instructions for FLIM-FRET-Calculation for Multi-Exponential
601 Donors, using a two-exponential decay for GFP. The lifetimes were initially estimated by

fitting the data using the Monte Carlo method and then by fitting the data using the Maximum Likely Hood Estimation (MLE). The amplitude weighted average donor lifetime with model parameter n=2 was used to calculate the average FRET-efficiency. FRET efficiency (E) was calculated by comparing the lifetime of the donor in the presence τDA or absence τD of the acceptor according to the following formula: $E = 1 - \frac{\tau DA}{\tau D}$. Data was analysed either by Student's t-test for pairwise comparisons, or by ANOVA with Tukey-kramer post-hoc analysis for multiple comparisons. Statistical significance was concluded when p-value was less than 0.05. Sample-specific details are listed in the figure legends.

FRAP analysis

For FRAP experiments we used leaves of *N. benthamiana* transiently expressing Citrine-LYM2, LYK4-RFP or LYK5-RFP treated for 30 min with chitin (500 µg/mL) or water (mock). FRAP was performed using a Leica TCS SP8X CLSM with a 63x/1.20 water immersion objective (Leica HC PL APO CS2 63×/1.20). To reduce scanning time the acquisition window was limited to 512 by 64 pixels. Citrine was excited at 514 nm and emissions detected between 527-550 nm. RFP was excited at 561 nm and emissions detected between 567-617 nm. ROIs were defined for plasmodesmata-localised Citrine-LYM2 and for PM-localised Citrine-LYM2, LYK4-RFP and LYK5-RFP. The FRAP protocol was as follows: 30 iterations were imaged at 0.095 sec/frame (pre-bleach); 15 (Citrine) or 60 (RFP) iterations at 0.095 sec/frame (bleach); and 50 iterations at 0.095 sec/frame followed by 120 iterations every 0.5 s (post-bleach). For bleach iterations the laser power was set to 100% and the FRAP booster was used.

Intensity data were normalised to the mean intensity of the first five frames and corrected for bleaching induced by pre- and post-bleach iterations. For the latter we collected non-bleached image acquisition decay curves. These data were themselves normalised to mean intensity of the first five frames and were fitted by a LOESS regression. Thus, all experimental FRAP data was corrected as follows:

$$I_{corr} = I_{norm} + \left(100 - I_{decay}\right) [\%]$$

I_{corr} is the corrected intensity, I_{norm} is the normalised intensity, I_{decay} is the modelled intensity from the acquisition decay curve.

Data was further transformed to set the bleach base-line to zero: thus

$$I_{final} = \frac{I_{corr} - I_{bleach}}{I_{pre-bleach}} * 100\ [\%]$$

I_{final} is the final intensity, I_{bleach} is the intensity at the last bleach interation, $I_{pre\text{-}bleach}$ is the mean of the pre-bleach values.

A LOESS curve was modelled to each dataset and each curve fit was sanity checked (Spira *et al.*, 2012). The intensity value at 60 s post-bleach was used as an approximation of the relative mobile fraction, adapted from Martiniere *et al.* (2012). Pairwise comparisons of estimated marginal means were performed in R 3.5.1 (R Core Team, 2018) using emmeans (Lenth et al., 2018; https://cran.r-project.org/web/packages/emmeans/index.html).

Co-immunoprecipitation

Proteins were isolated using an extraction buffer containing 50 mM Tris-HCl pH 7.5, 150 mM NaCl, 5mM dithiothreitol (DTT), protease inhibitor cocktail (Sigma) 1:100, phosphatase inhibitor (Sigma) 1:200, 1 mM phenylmethanesulfonyl fluoride (PMSF) and 0.5% IGEPAL® CA-630 (Sigma). For co-immunoprecipitation, GFP-Trap agarose beads (ChromoTek) were incubated with the protein samples for 2 hours at 4 °C with gentle agitation. Beads were then washed three times with a washing buffer containing 50 mM Tris-HCl pH 7.5, 150 mM NaCl, 5mM dithiothreitol, protease inhibitor cocktail 1:100, phosphatase inhibitor 1:200, 1 mM phenylmethanesulfonyl fluoride and 0.1% IGEPAL. After addition of Laemmli buffer (2×) containing 50 mM Tris-HCl pH 7, 5% SDS, 20% glycerol, 2% bromophenol blue, 5% β-mercaptoethanol, samples were boiled for 15 minutes at 95 °C. Protein samples were analysed by SDS-PAGE and transferred to Immuno-blot® PVDF membrane. Proteins were detected with α-GFP-HRP (Miltenyi Biotec, 130-091-833), α-Myc-HRP (Abcam, ab622928), α-HA-HRP (Abcam, ab173826), α-RFP-biotin (Abcam, ab34771) antibodies. α-RFP-biotin was detected using α -rabbit IgG–Alkaline Phosphatase (Sigma, a3687).

Plasmodesmata extraction

The plasmodesmal purification method from Arabidopsis suspension cultures cells was modified for use with mature leaf tissue. Four expanded 5-week-old *N. benthamiana* leaves, transiently expressing the desired construct, were ground in liquid nitrogen to a fine powder. The powder was ultrasonicated in extraction buffer (50 mM Tris-HCl pH 7.5, 150 mM NaCl, 1× cOmplete™ ULTRA EDTA-free protease inhibitors (Roche), 1 mM PMSF, 1% w/v PVP-

40kDa (Sigma)), followed by high-pressure homogenisation (EmulsiFlex B15, Avestin) to produce the "Total" fraction. Triton-X100 (0.5% v/v) was added to the resultant homogenate and the sample was centrifuged at 400*g* at 4°C to collect a crude cell wall extraction. Cell walls were washed five times with extraction buffer, and once in cellulase buffer (20 mM MES-KOH pH 5.5, 100mM NaCl, 1× cOmplete™ ULTRA EDTA-free protease inhibitors (Roche), 1 mM PMSF, 4.4% w/v mannitol). Washed cell wall material was resuspended in an equal volume of cellulase buffer with 2% (w/v) Cellulase R-10 (Yakult pharmaceuticals, Japan) and shaken at 37°C for one hour. Undigested cell wall material was removed by centrifugation at 2500*g* at 4°C. The supernatant was ultracentrifuged at 130,000*g* at 4°C to collect plasmodesmal membranes. The membrane pellet was resuspended in 50 µL resuspension buffer (50 mM Tris-HCl pH 7.5, 150 mM NaCl, 5 mM DTT, 1× cOmplete™ ULTRA EDTA-free protease inhibitors (Roche), 1 mM PMSF, 0.2% v/v IPEGAL® CA-630 (Sigma)) as a "PD" fraction. Protein extracts were boiled in Laemmli buffer and separated by 10% SDS-PAGE. Proteins were transferred to Immuno-blot® PVDF (0.2 µm, Bio-Rad) by semi-dry transfer. The membrane was probed with primary-conjugated HRP antibodies against HA (1:5000, ab173826, Abcam) and Myc (1:5000, ab62928, Abcam). HRP signal was developed with SuperSignal West Femto (ThermoFisher) and detected using ImageQuant LAS 500 (GE Healthcare).

ROS burst measurement

Leaf discs (4 mm in diameter) were immerged in in 96-well white plates (Greiner bio-one) containing sterile water overnight in the dark. The next day, the water was replaced by a solution containing 20 µg/mL HRP (Sigma), 17 µg/mL luminol (Sigma), and chitin (NaCoSy, 500 µg/mL) or water (mock). Integrated luminescence was measured using a luminometer (Varioskan Flash) for 40 minutes. The normality of each data set was assessed and confirmed by a Shapiro-Wilk test. Thus, a Student's t-test was applied for pairwise comparisons and significant differences were concluded when p-value was less than 0.05. Sample-specific details are listed in the figure legends.

Statistical analyses

Statistical analyses were performed using Genstat® version 18 or R 3.5.1. Details are in the relevant methods section and/or figure legends. n-values are detailed in Table S1.

693 **Acknowledgements**

694 The authors acknowledge access to the JIC Bioimaging Facility we thank the staff for their
695 assistance and training with the microscopes. The authors particularly thank Grant Calder and
696 Yvonne Stahl (University of Düsseldorf) for assistance in developing the FRET-FLIM
697 methods. *lyk3*, *lyk4* and *lyk5-2* seeds were provided by Gary Stacey. This work was funded
698 by: the Biotechnology and Biological Research Council (BB/L000466/1, CF;
699 BBS/E/J/000PR9796, CF); the European Research Council (grant 'INTERCELLAR', CF);
700 and the Gatsby Charitable Foundation (CZ). The authors thank Caroline Dean for discussions
701 and critical reading of the manuscript.

702

703

References

Benitez-Alfonso Y, Faulkner C, Pendle A, Miyashima S, Helariutta Y, Maule A. 2013. Symplastic intercellular connectivity regulates lateral root patterning. *Dev Cell* **26**:136–147. doi:10.1016/j.devcel.2013.06.010

Bucherl CA, Jarsch IK, Schudoma C, Segonzac C, Mbengue M, Robatzek S, MacLean D, Ott T, Zipfel C. 2017. Plant immune and growth receptors share common signalling components but localise to distinct plasma membrane nanodomains. *Elife* **6**. doi:10.7554/eLife.25114

Cao Y, Liang Y, Tanaka K, Nguyen CT, Jedrzejczak RP, Joachimiak A, Stacey G. 2014. The kinase LYK5 is a major chitin receptor in Arabidopsis and forms a chitin-induced complex with related kinase CERK1. *Elife* **3**. doi:10.7554/eLife.03766

Cui W, Lee JY. 2016. Arabidopsis callose synthases CalS1/8 regulate plasmodesmal permeability during stress. *Nat Plants* **2**:16034. doi:10.1038/nplants.2016.34

Danila FR, Quick WP, White RG, Kelly S, von Caemmerer S, Furbank RT. 2018. Multiple mechanisms for enhanced plasmodesmata density in disparate subtypes of C4 grasses. *J Exp Bot* **69**:1135–1145. doi:10.1093/jxb/erx456

Dubiella U, Seybold H, Durian G, Komander E, Lassig R, Witte CP, Schulze WX, Romeis T. 2013. Calcium-dependent protein kinase/NADPH oxidase activation circuit is required for rapid defense signal propagation. *Proc Natl Acad Sci U S A* **110**:8744–8749. doi:10.1073/pnas.1221294110

Erwig J, Ghareeb H, Kopischke M, Hacke R, Matei A, Petutschnig E, Lipka V. 2017. Chitin-induced and CHITIN ELICITOR RECEPTOR KINASE1 (CERK1) phosphorylation-dependent endocytosis of Arabidopsis thalia na LYSIN MOTIF-CONTAINING RECEPTOR-LIKE KINASE5 (LYK5). *New Phytol* **215**:382–396. doi:10.1111/nph.14592

Faulkner C, Akman OE, Bell K, Jeffree C, Oparka K. 2008. Peeking into pit fields: a multiple twinning model of secondary plasmodesmata formation in tobacco. *Plant Cell* **20**:1504–1518. doi:10.1105/tpc.107.056903

Faulkner C, Petutschnig E, Benitez-Alfonso Y, Beck M, Robatzek S, Lipka V, Maule AJ. 2013. LYM2-dependent chitin perception limits molecular flux via plasmodesmata. *Proc Natl Acad Sci U S A* **110**:9166–9170. doi:10.1073/pnas.1203458110

Fernandez-Calvino L, Faulkner C, Walshaw J, Saalbach G, Bayer E, Benitez-Alfonso Y, Maule A. 2011. Arabidopsis plasmodesmal proteome. *PLoS One* **6**:e18880. doi:10.1371/journal.pone.0018880

Grison MS, Brocard L, Fouillen L, Nicolas W, Wewer V, Dormann P, Nacir H, Benitez-Alfonso Y, Claverol S, Germain V, Boutte Y, Mongrand S, Bayer EM. 2015. Specific membrane lipid composition is important for plasmodesmata function in Arabidopsis. *Plant Cell* **27**:1228–1250. doi:10.1105/tpc.114.135731

Gronnier J, Gerbeau-Pissot P, Germain V, Mongrand S, Simon-Plas F. 2018. Divide and Rule: Plant Plasma Membrane Organization. *Trends Plant Sci* **23**:899–917. doi:10.1016/j.tplants.2018.07.007

Hayafune M, Berisio R, Marchetti R, Silipo A, Kayama M, Desaki Y, Arima S, Squeglia F,

Ruggiero A, Tokuyasu K, Molinaro A, Kaku H, Shibuya N. 2014. Chitin-induced activation of immune signalling by the rice receptor CEBiP relies on a unique sandwich-type dimerization. *Proc Natl Acad Sci U S A* **111**:E404-13. doi:10.1073/pnas.1312099111

Hayashi F, Smith KD, Ozinsky A, Hawn TR, Yi EC, Goodlett DR, Eng JK, Akira S, Underhill DM, Aderem A. 2001. The innate immune response to bacterial flagellin is mediated by Toll-like receptor 5. *Nature* **410**:1099–1103. doi:10.1038/35074106

Hillmer RA, Tsuda K, Rallapalli G, Asai S, Truman W, Papke MD, Sakakibara H, Jones JDG, Myers CL, Katagiri F. 2017. The highly buffered Arabidopsis immune signalling network conceals the functions of its components. *PLoS Genet* **13**:e1006639. doi:10.1371/journal.pgen.1006639

Hunter K, Kimura S, Rokka A, Tran C, Toyota M, Kukkonen JP, Wrzaczek M. 2019. CRK2 enhances salt tolerance by regulating callose deposition in connection with PLDα1. *bioRxiv* 487009. doi:10.1101/487009

Kadota Y, Liebrand TWH, Goto Y, Sklenar J, Derbyshire P, Menke FLH, Torres MA, Molina A, Zipfel C, Coaker G, Shirasu K. 2018. Quantitative phosphoproteomic analysis reveals common regulatory mechanisms between effector- and PAMP-triggered immunity in plants. *New Phytol*. doi:10.1111/nph.15523

Kadota Y, Sklenar J, Derbyshire P, Stransfeld L, Asai S, Ntoukakis V, Jones JD, Shirasu K, Menke F, Jones A, Zipfel C. 2014. Direct regulation of the NADPH oxidase RBOHD by the PRR-associated kinase BIK1 during plant immunity. *Mol Cell* **54**:43–55. doi:10.1016/j.molcel.2014.02.021

Kaku H, Nishizawa Y, Ishii-Minami N, Akimoto-Tomiyama C, Dohmae N, Takio K, Minami E, Shibuya N. 2006. Plant cells recognize chitin fragments for defense signalling through a plasma membrane receptor. *Proc Natl Acad Sci U S A* **103**:11086–11091. doi:10.1073/pnas.0508882103

Kofoed EM, Vance RE. 2011. Innate immune recognition of bacterial ligands by NAIPs determines inflammasome specificity. *Nature* **477**:592–595. doi:10.1038/nature10394

Lee J-YY, Wang X, Cui W, Sager R, Modla S, Czymmek K, Zybaliov B, van Wijk K, Zhang C, Lu H, Lakshmanan V. 2011. A Plasmodesmata-Localized Protein Mediates Crosstalk between Cell-to-Cell Communication and Innate Immunity in Arabidopsis. *Plant Cell* **23**:3353–3373. doi:10.1105/tpc.111.087742

Li L, Li M, Yu L, Zhou Z, Liang X, Liu Z, Cai G, Gao L, Zhang X, Wang Y, Chen S, Zhou JM. 2014. The FLS2-associated kinase BIK1 directly phosphorylates the NADPH oxidase RbohD to control plant immunity. *Cell Host Microbe* **15**:329–338. doi:10.1016/j.chom.2014.02.009

Liang P, Stratil TF, Popp C, Marin M, Folgmann J, Mysore KS, Wen J, Ott T. 2018. Symbiotic root infections in Medicago truncatula require remorin-mediated receptor stabilization in membrane nanodomains. *Proc Natl Acad Sci U S A* **115**:5289–5294. doi:10.1073/pnas.1721868115

Liao D, Cao Y, Sun X, Espinoza C, Nguyen CT, Liang Y, Stacey G. 2017. Arabidopsis E3 ubiquitin ligase PLANT U-BOX13 (PUB13) regulates chitin receptor LYSIN MOTIF RECEPTOR KINASE5 (LYK5) protein abundance. *New Phytol*. doi:10.1111/nph.14472

789 Lim GH, Shine MB, de Lorenzo L, Yu K, Cui W, Navarre D, Hunt AG, Lee JY, Kachroo A,
790 Kachroo P. 2016. Plasmodesmata Localizing Proteins Regulate Transport and Signaling
791 during Systemic Acquired Immunity in Plants. *Cell Host Microbe* **19**:541–549.
792 doi:10.1016/j.chom.2016.03.006

793 Lingwood D, Simons K. 2010. Lipid rafts as a membrane-organizing principle. *Science (80-)*
794 **327**:46–50. doi:10.1126/science.1174621

795 Malinsky J, Opekarova M, Grossmann G, Tanner W. 2013. Membrane microdomains, rafts,
796 and detergent-resistant membranes in plants and fungi. *Annu Rev Plant Biol* **64**:501–
797 529. doi:10.1146/annurev-arplant-050312-120103

798 Martiniere A, Lavagi I, Nageswaran G, Rolfe DJ, Maneta-Peyret L, Luu DT, Botchway SW,
799 Webb SE, Mongrand S, Maurel C, Martin-Fernandez ML, Kleine-Vehn J, Friml J,
800 Moreau P, Runions J. 2012. Cell wall constrains lateral diffusion of plant plasma-
801 membrane proteins. *Proc Natl Acad Sci U S A* **109**:12805–12810.
802 doi:10.1073/pnas.1202040109

803 Miya A, Albert P, Shinya T, Desaki Y, Ichimura K, Shirasu K, Narusaka Y, Kawakami N,
804 Kaku H, Shibuya N. 2007. CERK1, a LysM receptor kinase, is essential for chitin
805 elicitor signalling in Arabidopsis. *Proc Natl Acad Sci U S A* **104**:19613–19618.
806 doi:10.1073/pnas.0705147104

807 Mori IC, Murata Y, Yang Y, Munemasa S, Wang YF, Andreoli S, Tiriac H, Alonso JM,
808 Harper JF, Ecker JR, Kwak JM, Schroeder JI. 2006. CDPKs CPK6 and CPK3 function
809 in ABA regulation of guard cell S-type anion- and Ca(2+)-permeable channels and
810 stomatal closure. *PLoS Biol* **4**:e327. doi:10.1371/journal.pbio.0040327

811 Mueller TD, Nickel J. 2012. Promiscuity and specificity in BMP receptor activation. *FEBS*
812 *Lett* **586**:1846–1859. doi:10.1016/j.febslet.2012.02.043

813 Ott T. 2017. Membrane nanodomains and microdomains in plant-microbe interactions. *Curr*
814 *Opin Plant Biol* **40**:82–88. doi:10.1016/j.pbi.2017.08.008

815 Pan L, Fu T-M, Zhao W, Zhao L, Chen W, Qiu C, Liu W, Liu Z, Piai A, Fu Q, Chen S, Wu
816 H, Chou JJ. 2019. Higher-Order Clustering of the Transmembrane Anchor of DR5
817 Drives Signaling. *Cell* **176**:1477–1489.e14. doi:10.1016/J.CELL.2019.02.001

818 Perraki A, Gronnier J, Gouguet P, Boudsocq M, Deroubaix AF, Simon V, German-Retana S,
819 Legrand A, Habenstein B, Zipfel C, Bayer E, Mongrand S, Germain V. 2018. REM1.3's
820 phospho-status defines its plasma membrane nanodomain organization and activity in
821 restricting PVX cell-to-cell movement. *PLoS Pathog* **14**:e1007378.
822 doi:10.1371/journal.ppat.1007378

823 Petutschnig EK, Stolze M, Lipka U, Kopischke M, Horlacher J, Valerius O, Rozhon W, Gust
824 AA, Kemmerling B, Poppenberger B, Braus GH, Nurnberger T, Lipka V. 2014. A novel
825 Arabidopsis CHITIN ELICITOR RECEPTOR KINASE 1 (CERK1) mutant with
826 enhanced pathogen-induced cell death and altered receptor processing. *New Phytol*
827 **204**:955–967. doi:10.1111/nph.12920

828 Płóciennikowska A, Hromada-Judycka A, Borzęcka K, Kwiatkowska K. 2015. Co-operation
829 of TLR4 and raft proteins in LPS-induced pro-inflammatory signalling. *Cell Mol Life*
830 *Sci* **72**:557–581. doi:10.1007/s00018-014-1762-5

831 Rao S, Zhou Z, Miao P, Bi G, Hu M, Wu Y, Feng F, Zhang X, Zhou JM. 2018. Roles of

Receptor-Like Cytoplasmic Kinase VII Members in Pattern-Triggered Immune Signaling. *Plant Physiol* **177**:1679–1690. doi:10.1104/pp.18.00486

Ren H, Willige BC, Jaillais Y, Geng S, Park MY, Gray WM, Chory J. 2019. BRASSINOSTEROID-SIGNALING KINASE 3, a plasma membrane-associated scaffold protein involved in early brassinosteroid signalling. *PLOS Genet* **15**:e1007904.

Rinne PL, Welling A, Vahala J, Ripel L, Ruonala R, Kangasjarvi J, van der Schoot C. 2011. Chilling of dormant buds hyperinduces FLOWERING LOCUS T and recruits GA-inducible 1,3-beta-glucanases to reopen signal conduits and release dormancy in Populus. *Plant Cell* **23**:130–146. doi:10.1105/tpc.110.081307

Rinne PLH, Paul LK, van der Schoot C. 2018. Decoupling photo- and thermoperiod by projected climate change perturbs bud development, dormancy establishment and vernalization in the model tree Populus. *BMC Plant Biol* **18**:220. doi:10.1186/s12870-018-1432-0

Scott FL, Stec B, Pop C, Dobaczewska MK, Lee JJ, Monosov E, Robinson H, Salvesen GS, Schwarzenbacher R, Riedl SJ. 2008. The Fas–FADD death domain complex structure unravels signalling by receptor clustering. *Nature* **457**:1019.

Spira F, Mueller NS, Beck G, von Olshausen P, Beig J, Wedlich-Soldner R. 2012. Patchwork organization of the yeast plasma membrane into numerous coexisting domains. *Nat Cell Biol* **14**:640–648. doi:10.1038/ncb2487

Stahl Y, Grabowski S, Bleckmann A, Kuhnemuth R, Weidtkamp-Peters S, Pinto KG, Kirschner GK, Schmid JB, Wink RH, Hulsewede A, Felekyan S, Seidel CA, Simon R. 2013. Moderation of Arabidopsis root stemness by CLAVATA1 and ARABIDOPSIS CRINKLY4 receptor kinase complexes. *Curr Biol* **23**:362–371. doi:10.1016/j.cub.2013.01.045

Stegmann M, Monaghan J, Smakowska-Luzan E, Rovenich H, Lehner A, Holton N, Belkhadir Y, Zipfel C. 2017. The receptor kinase FER is a RALF-regulated scaffold controlling plant immune signalling. *Science (80-)* **355**:287–289. doi:10.1126/science.aal2541

Tilsner J, Nicolas W, Rosado A, Bayer EM. 2016. Staying Tight: Plasmodesmal Membrane Contact Sites and the Control of Cell-to-Cell Connectivity in Plants. *Annu Rev Plant Biol* **67**:337–364. doi:10.1146/annurev-arplant-043015-111840

Torres MA, Dangl JL, Jones JD. 2002. Arabidopsis gp91phox homologues AtrbohD and AtrbohF are required for accumulation of reactive oxygen intermediates in the plant defense response. *Proc Natl Acad Sci U S A* **99**:517–522. doi:10.1073/pnas.012452499

Vaten A, Dettmer J, Wu S, Stierhof YD, Miyashima S, Yadav SR, Roberts CJ, Campilho A, Bulone V, Lichtenberger R, Lehesranta S, Mahonen AP, Kim JY, Jokitalo E, Sauer N, Scheres B, Nakajima K, Carlsbecker A, Gallagher KL, Helariutta Y. 2011. Callose biosynthesis regulates symplastic trafficking during root development. *Dev Cell* **21**:1144–1155. doi:10.1016/j.devcel.2011.10.006

Veronese P, Nakagami H, Bluhm B, Abuqamar S, Chen X, Salmeron J, Dietrich RA, Hirt H, Mengiste T. 2006. The membrane-anchored BOTRYTIS-INDUCED KINASE1 plays distinct roles in Arabidopsis resistance to necrotrophic and biotrophic pathogens. *Plant Cell* **18**:257–273. doi:10.1105/tpc.105.035576

875 Wan J, Tanaka K, Zhang XC, Son GH, Brechenmacher L, Nguyen TH, Stacey G. 2012.
876 LYK4, a lysin motif receptor-like kinase, is important for chitin signalling and plant
877 innate immunity in Arabidopsis. *Plant Physiol* **160**:396–406.
878 doi:10.1104/pp.112.201699

879 Wang L, Li H, Lv X, Chen T, Li R, Xue Y, Jiang J, Jin B, Baluška F, Šamaj J, Wang X, Lin
880 J. 2015. Spatiotemporal Dynamics of the BRI1 Receptor and its Regulation by
881 Membrane Microdomains in Living Arabidopsis Cells. *Mol Plant* **8**:1334–1349.
882 doi:https://doi.org/10.1016/j.molp.2015.04.005

883 Wang X, Sager R, Cui W, Zhang C, Lu H, Lee JY. 2013. Salicylic acid regulates
884 Plasmodesmata closure during innate immune responses in Arabidopsis. *Plant Cell*
885 **25**:2315–2329. doi:10.1105/tpc.113.110676

886 Willmann R, Lajunen HM, Erbs G, Newman M-A, Kolb D, Tsuda K, Katagiri F, Fliegmann
887 J, Bono J-J, Cullimore J V, Jehle AK, Goetz F, Kulik A, Molinaro A, Lipka V, Gust
888 AA, Nuernberger T. 2011. Arabidopsis lysin-motif proteins LYM1 LYM3 CERK1
889 mediate bacterial peptidoglycan sensing and immunity to bacterial infection. *Proc Natl*
890 *Acad Sci U S A* **108**:19824–19829. doi:10.1073/pnas.1112862108

891 Winter D, Vinegar B, Nahal H, Ammar R, Wilson G V, Provart NJ. 2007. An "Electronic
892 Fluorescent Pictograph" browser for exploring and analyzing large-scale biological data
893 sets. *PLoS One* **2**:e718. doi:10.1371/journal.pone.0000718

894 Xu B, Cheval C, Laohavisit A, Hocking B, Chiasson D, Olsson TSG, Shirasu K, Faulkner C,
895 Gilliham M. 2017. A calmodulin-like protein regulates plasmodesmata closure during
896 bacterial immune responses. *New Phytol* **215**:77–84. doi:10.1111/nph.14599

897 Yamada K, Yamaguchi K, Shirakawa T, Nakagami H, Mine A, Ishikawa K, Fujiwara M,
898 Narusaka M, Narusaka Y, Ichimura K, Kobayashi Y, Matsui H, Nomura Y, Nomoto M,
899 Tada Y, Fukao Y, Fukamizo T, Tsuda K, Shirasu K, Shibuya N, Kawasaki T. 2016. The
900 Arabidopsis CERK1-associated kinase PBL27 connects chitin perception to MAPK
901 activation. *EMBO J* **35**:2468 LP-2483. doi:10.15252/embj.201694248

902 Yoo SD, Cho YH, Sheen J. 2007. Arabidopsis mesophyll protoplasts: a versatile cell system
903 for transient gene expression analysis. *Nat Protoc* **2**:1565–1572.
904 doi:10.1038/nprot.2007.199

905 Zhao Y, Yang J, Shi J, Gong Y-N, Lu Q, Xu H, Liu L, Shao F. 2011. The NLRC4
906 inflammasome receptors for bacterial flagellin and type III secretion apparatus. *Nature*
907 **477**:596–600. doi:10.1038/nature10510

908

909

910 **Figures and Tables**

911

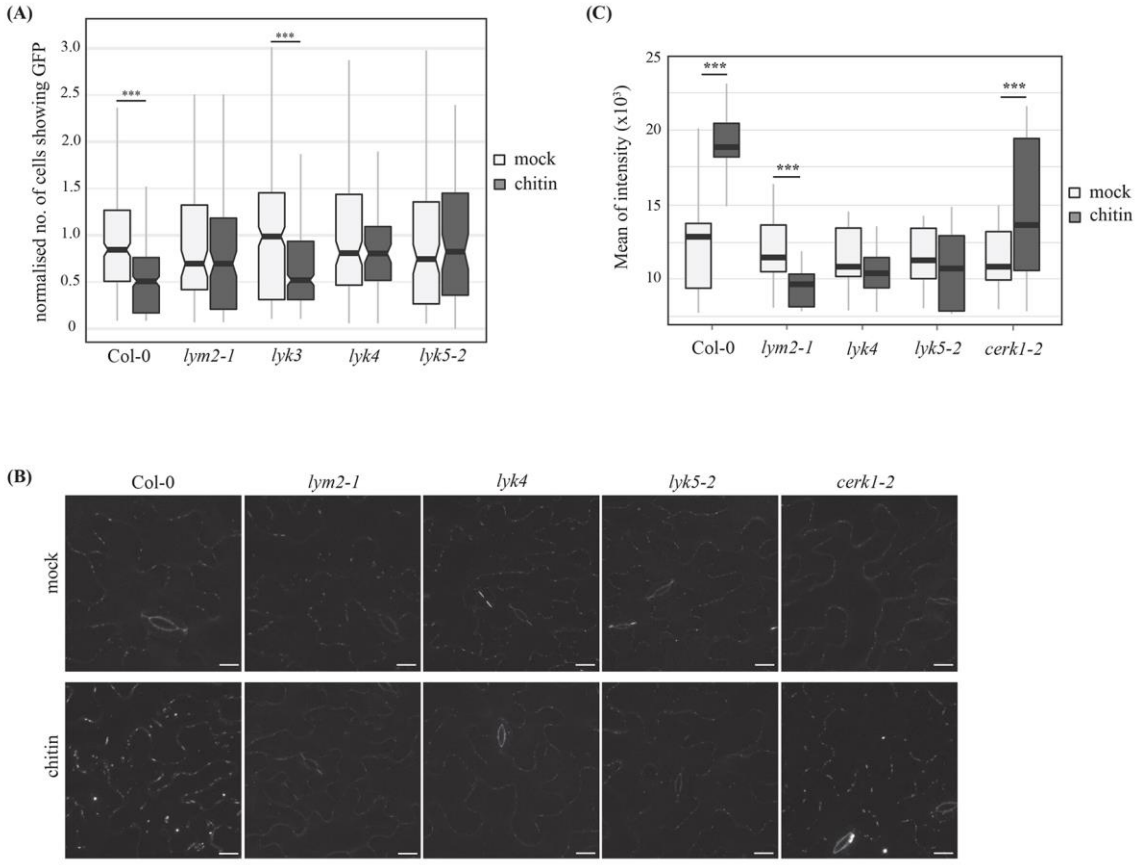

912 Figure 1

913 **Figure 1. LYK4 and LYK5 regulate plasmodesmal permeability in response to chitin**

914 (A) Microprojectile bombardment into leaf tissue of 5–6-week-old Arabidopsis shows that
915 Col-0 and *lyk3* but not *lym2-1*, *lyk4* and *lyk5-2* exhibit reduced flux of GFP to neighbouring
916 cells in response to chitin. Data was collected from 6 biological replicates and the number of
917 cells showing GFP has been normalised to the mean of the mock-treated data within
918 genotypes. This data is summarised in box-plots in which the line within the box marks the
919 median, the box signifies the upper and lower quartiles, the whiskers represent the minimum
920 and maximum within 1.5 × interquartile range. Notches represent approximate 95%
921 confidence intervals. Asterisks indicate statistical significance compared to control
922 conditions ($n \geq 85$, ***p-value < 0.001). (B) Confocal images of aniline blue stained
923 plasmodesmal callose in leaves of 5–6-week-old Col-0 plants, as well as *lym2-1*, *lyk4*, *lyk5-2*,
924 and *cerk1-2* mutants. Images were acquired 30 min post-infiltration with water or chitin.
925 Scale bars are 15 µm. (C) Quantification of plasmodesmata-associated fluorescence of aniline

926 blue stained callose using automated image analysis. Col-0 and the *cerk1-2* mutant show an
927 increase in aniline blue stained plasmodesmal callose 30 min post-chitin treatment. In *lym2-1*,
928 *lyk4* and *lyk5-2* this response is not detected. This correlates with the flux phenotype and
929 identifies that chitin-triggered plasmdesmata closure is caused by callose deposition at
930 plasmodesmata. The fluorescence intensity is summarised in box-plots in which the line
931 within the box marks the median, the box signifies the upper and lower quartiles, the
932 minimum and maximum within 1.5 × interquartile range. Data was analysed by pairwise
933 Students' t-test comparing mock to chitin treated tissue within genotypes ($n \geq 31$, ***p-value
934 < 0.001).

935

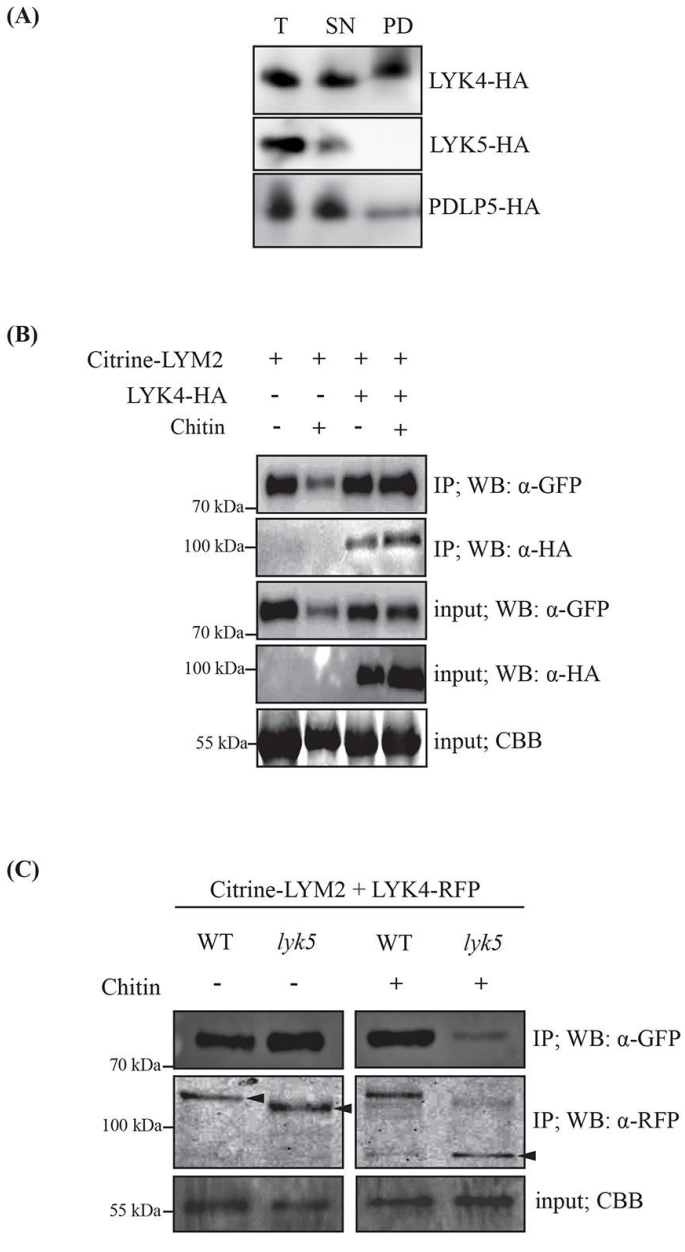

Figure 2

936

937 **Figure 2. LYK4 is detected in plasmodesmata and associates with LYM2**

938 (A) Western blot analysis of purified plasmodesmata fractions from *N. benthamiana* tissue
939 co-expressing LYK4-HA, LYK5-HA or PDLP5-HA. Total (T; extracts from ground tissue),
940 supernatant (SN; all cellular material excluding cell walls) and plasmodesmatal (PD;
941 membranes released from purified cell walls) extracts were separated by SDS-PAGE and
942 Western blots were probed with anti-HA and to determine the presence of LYK4-HA, LYK5-
943 HA and PDLP5-HA in each fraction. Experiments were repeated four times with similar

944 results. (B) Western blot analysis of immunoprecipitated protein extracts from *N.*
945 *benthamiana* tissue expressing Citrine-LYM2 and LYK4-HA. LYK4-HA is detected in
946 samples purified from membrane fractions by immunoprecipitation of Citrine-LYM2 with
947 GFP-trap beads. Input and immunoprecipitated (IP) samples were probed α-GFP and α-HA
948 antibodies as indicated. CBB, Coomassie brilliant blue. Size standards are indicated to the left
949 of the panel. Experiments were repeated three times with similar results. (C) Western blot
950 analysis of immunoprecipitated protein extracts from Arabidopsis protoplasts expressing
951 Citrine-LYM2 and LYK4-HA. LYK4-HA is detected in samples purified from membrane
952 fractions by immunoprecipitation of Citrine-LYM2 with GFP-trap beads from both Col-0 and
953 *lyk5-2* protoplasts. Input and immunoprecipitated (IP) samples were probed α-GFP and α-HA
954 antibodies as indicated. LYK4-HA bands of different sizes are indicated by arrowheads.
955 CBB, Coomassie brilliant blue. Size standards are indicated to the left of the panel.
956 Experiments were repeated three times with similar results.

957

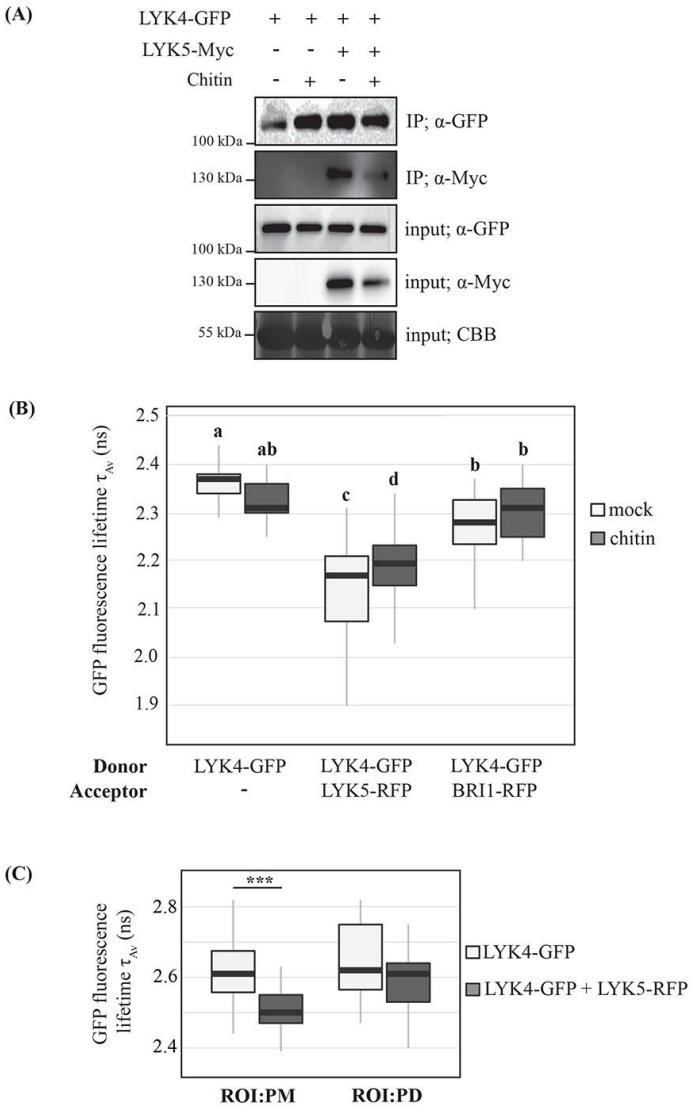

Figure 3

Figure 3. LYK5 dynamically associates with LYK4 in the PM

(A) Western blot analysis of immunoprecipitated protein extracts from *N. benthamiana* tissue expressing LYK4-GFP and LYK5-Myc. LYK4-GFP was immunoprecipitated from membrane fractions and western blots of input and immunoprecipitated extracts were probed with α-GFP and α-Myc to detect LYK4-GFP and LYK5-Myc respectively. Coomassie brilliant blue (CBB) stained membranes serve as a loading control. Size standards are indicated to the left of the panel. Experiments were repeated three times with similar results. (B) FRET-FLIM analysis of LYK4-GFP in the presence of acceptors LYK5-RFP or BRI1-

RFP, and the presence and absence of chitin. Fluorescence lifetime was measured in *N. benthamiana* tissue transiently co-expressing the indicated constructs as donors or acceptors. Box-plots represent GFP fluorescence-weighted average lifetime (τ_{Av}, ns) fitted with a double-exponential model: the line within the box marks the median, the box signifies the upper and lower quartiles, the whiskers represent the minimum and maximum within 1.5 × interquartile range. Data was analysed by ANOVA with a post-hoc Tukey multiple comparison of means (p-value <0.01, n ≥19). Samples with the same letter code are not significantly different. (C) FRET-FLIM analysis of LYK4-GFP at the plasmodesmal PM and the PM in the presence and absence of LYK5-RFP RFP. Fluorescence lifetime was measured in in *N.benthamiana* tissue transiently co-expressing the noted constructs. Plasmodesmata were marked by co-expression of Citrine-LYM2 and ROI were defined around plasmodesmata (PD) and in the PM for analysis. Box-plots represent GFP fluorescence-weighted average lifetime (τ_{Av}, ns) fitted with a double-exponential model: the line within the box marks the median, the box signifies the upper and lower quartiles, the whiskers represent the minimum and maximum within 1.5 × interquartile range. Data was analysed by a Students' t-test in which the lifetime of LYK4-GFP was compared in the absence and presence of LYK5-RFP for both ROIs. Asterisks indicate statistical significance compared to control conditions (n≥ 27, p-value < 0.001).

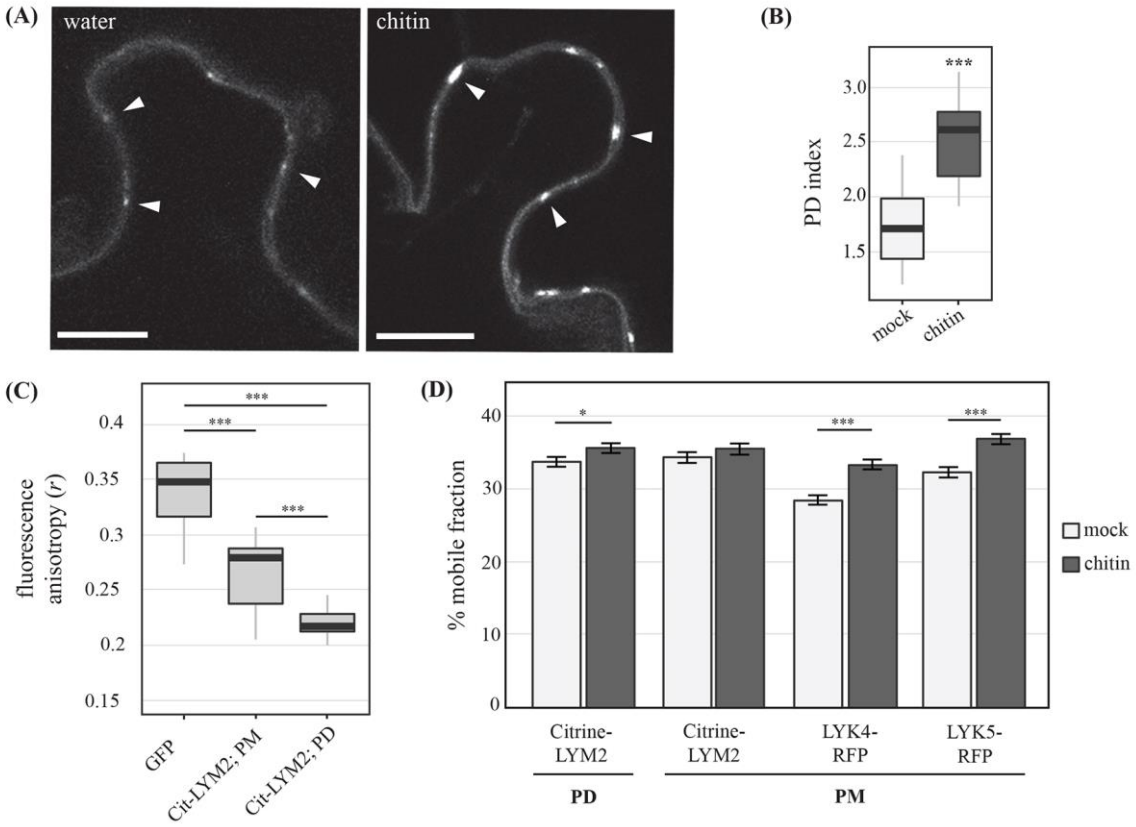

Figure 4

986

987 **Figure 4. LYM2 accumulates at PD in response to chitin**

988 (A) Single plane confocal images of *N.benthamiana* tissue expressing Citrine-LYM2 before
989 and after chitin treatment. Left panel shows Citrine-LYM2 in water-treated tissue and the
990 right shows Citrine-LYM 30 min post chitin treatment. Arrowheads indicate example
991 plasmodesmata. Scale bars, 10 µm. (B) Quantification of the PD index of Citrine-LYM2 at
992 PD in *N.benthamiana* after mock and chitin treatments. Data was analysed with a Students t-
993 test (***p-value < 0.001, n=31). (C) Fluorescence anisotropy (*r*) of cytosolic GFP, PM
994 located Citrine-LYM2 and plasmodesmata-located (PD) Citrine-LYM2. Data was analysed
995 pairwise by a Students' t-test (***p-value <0.001, GFP: n=11, Citrine-LYM2: n=21). (D) %
996 mobile fraction of LYM2, LYK4 and LYK5 as measured by FRAP assays. For Citrine-
997 LYM2 FRAP measurements were taken for the plasmodesmata-located (PD) and PM-located
998 pools of receptor. For LYK4-RFP and LYK5-RFP FRAP measurements were taken in the
999 PM. Data was analysed by LOESS regression and estimated marginal means analysis, error
1000 bars are standard error (***p-value <0.001, n ≥43).

1001

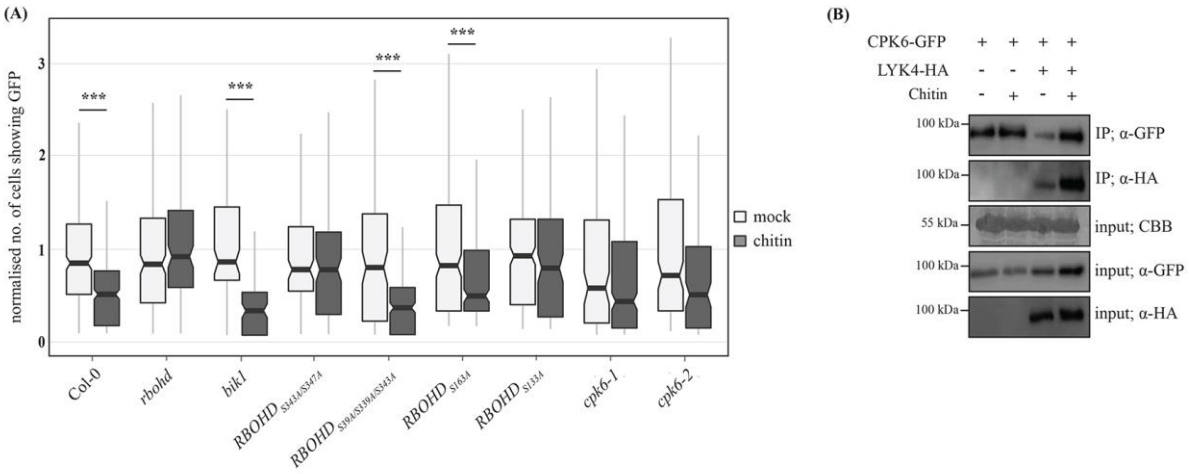

Figure 5

Figure 5. CPK-dependent phosphorylation of RBOHD is required for plasmodesmata closure in response to chitin

(A) Microprojectile bombardment into leaf tissue shows that *rbohd* mutants do not show a reduction in GFP flux to neighbouring cells in response to chitin. The *bik1* mutant, and RBOHD phosphosite mutant variants *S39A/S339A/S343A* and *S163A* exhibit a similar reduction in movement of GFP to neighbouring cells in response to chitin. By contrast, the RBOHD phosphosite mutant variants *S343A/S347A* and *S133A*, and the *CPK6* mutants *cpk6-1* and *cpk6-2* show no reduction in GFP flux to neighbouring cells in response to chitin. Data was collected from 6 biological replicates and the number of cells showing GFP has been normalised to the mean of the mock data within genotypes. This data is summarised in box-plots in which the line within the box marks the median, the box signifies the upper and lower quartiles, the minimum and maximum within 1.5 × interquartile range. Notches represent approximate 95% confidence intervals. Data has been analysed by a Students' t-test, or by a Mann-Whitney U-test for non-normal data ($n \geq 93$, ***p-value < 0.001). (B) LYK4 co-immunoprecipitates with CPK6 in *N. benthamiana*. CPK6-GFP was transiently co-expressed with LYK4-HA in *N. benthamiana* leaf tissue and CPK6-GFP was immunoprecipitated using GFP-trap beads. Input and immunoprecipitated (IP) samples were analysed by western blots probed with α-GFP and α-HA. Coomassie brilliant blue (CBB) staining of membranes serves as a loading control. The experiment was repeated three times with similar results.

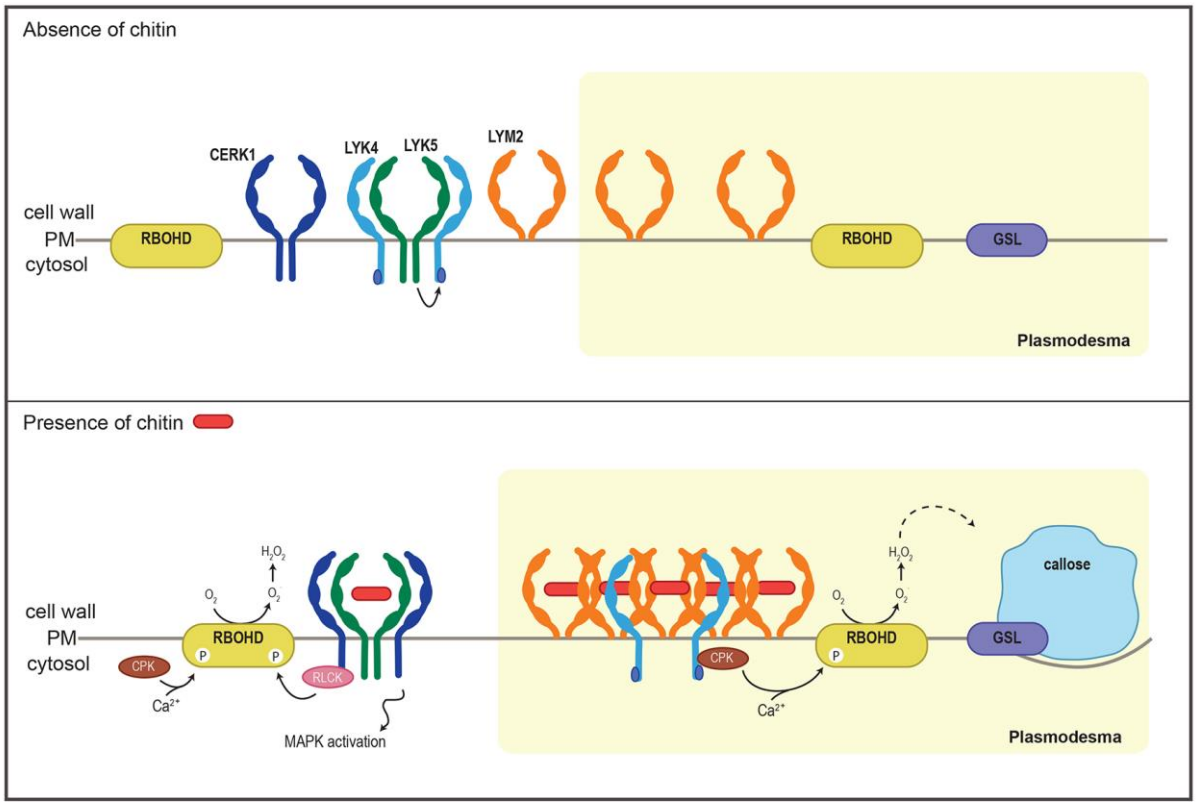

Figure 6

Figure 6. Model for LYM2-mediated chitin signalling in the plasmodesmal PM.

This cartoon describes our proposal for some of the key elements of LysM signalling in the PM and plasmodesmal PM in response to chitin perception. The top panel represents functional, interactions under control conditions. Here, LYK5 (green) interacts with LYK4 (light blue) and mediates modification of LYK4 in the PM, and LYM2 (orange) is distributed throughout the PM and the plasmodesmal PM. In response to chitin (lower panel), LYK4 and LYK5 dissociate. LYK5 interacts with CERK1 (dark blue) to mediate signalling at the PM, and LYM2 accumulates at plasmodesmata where it forms a higher order complex. This complex recruits LYK4 and CPK6 (brown) which phosphorylates RBOHD (yellow) and induces callose (blue) synthesis via a glucan-synthase like enzyme (GSL, purple) to close PD.

Table 1. FRET efficiencies of LYK4-GFP in the presence and absence of the acceptor-RFP. The mean of FRET efficiency is expressed in percentage (%). PM, plasma membrane; PD, plasmodesmata; SE, standard error.

Localisation	Donor	Acceptor	Treatment	Additional Construct	FRET efficiency (%)	SE
PM	LYK4-GFP	_	_	_	_	_
PM	LYK4-GFP	LYK5-RFP	_	_	10.65	0.02
PM	LYK4-GFP	BRI1-RFP	_	_	3.76	0.43
PM	LYK4-GFP	_	chitin	_	2.05	0.46
PM	LYK4-GFP	LYK5-RFP	chitin	_	7.20	0.53
PM	LYK4-GFP	BRI1-RFP	chitin	_	2.74	0.56
PD	LYK4-GFP	_	_	Citrine-LYM2	_	_
PD	LYK4-GFP	LYK5-RFP	_	Citrine-LYM2	2.50	0.55
PM	LYK4-GFP	_	_	Citrine-LYM2	_	_
PM	LYK4-GFP	LYK5-RFP	_	Citrine-LYM2	4.69	0.55

1041 **Table 2.** Primer sequences used in RT-PCR analysis of *LYSM-RK*s.

Gene	**Primer Sequences (5'-3')**
ACTIN2	F: ATGGCTGAGGCTGATGATATTCAAC R: CCAGGAATCGTTCACAGAAAATGTTTC
CERK1	F: ATGAAGCTAAAGATTTCTCTAATCGCTCCG R: GTCAGTCTTATGTCCGGCCGGTAG
LYK2	F: ATGGCTGTTTCAGTTAGTAAGC R: CCTTTGGTAAAGAAGAGTAGTATAATAG
LYK3	F: GCAAAGAGTGGTAGTCATGTGCC R: GTGGTCTAGTCCAAGGAAGATAA
LYK4	F: CCACAATCGGTTTCTCCTCCTCCATTGTC R: CTACGCAGAACTGGGAAGAATCGTCGTAC
LYK5	F: TTCTGGTCTCAACCACCGTAC R: CATCCGTCTCTCAGGTTTCTG

1042

1043

1044 **Supplementary Data**

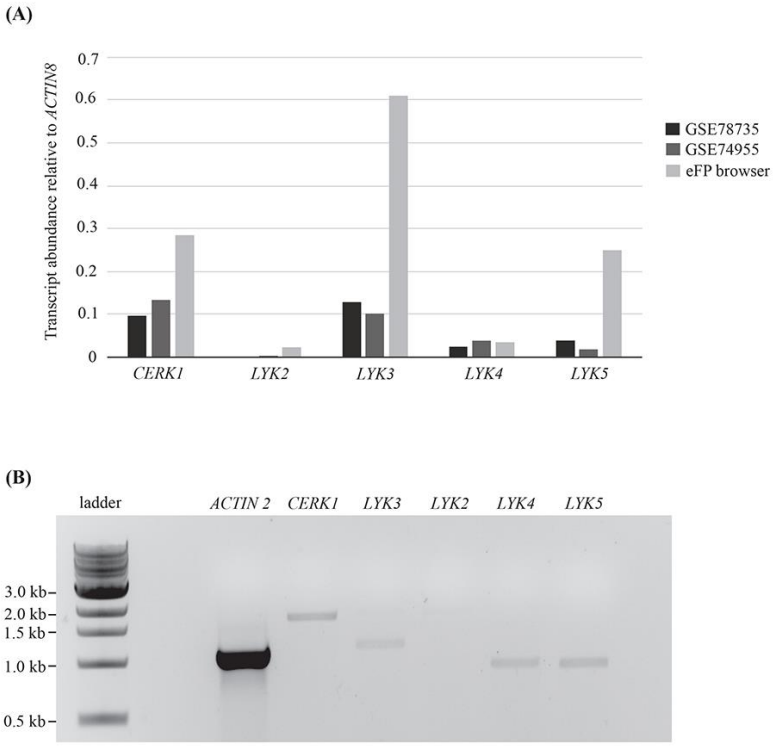

Figure S1

1045

1046 **Figure S1. *LYK2* is not detected in mature leaves.** (A) Publically available gene expression
1047 data from RNAseq (GSE78735 Hillmer *et al.*, 2017; GSE74955, Yamada *et al.*, 2016) and
1048 microarray experiments (eFP browser, Winter *et al.*, 2007) showing mRNA abundance of
1049 *LYK* family members relative to *ACTIN8*. The experimental data sets are indicated. (B) Semi-
1050 quantitative transcript abundance of *LYSM-RKs* in 5–6-week-old Arabidopsis leaf tissue.
1051 Transcript abundance was detected by RT-PCR and *ACTIN2* was used as an internal control.
1052 The primers used for RT-PCR are listed in the supplemental data (Table 2). RT-PCR reaction
1053 with these primers give the following sizes: ACTIN2, 1131bp; CERK1, 1854bp; LYK2,
1054 1960bp; LYK3, 1275bp; LYK4, 1083bp; LYK5, 1082bp.

1055

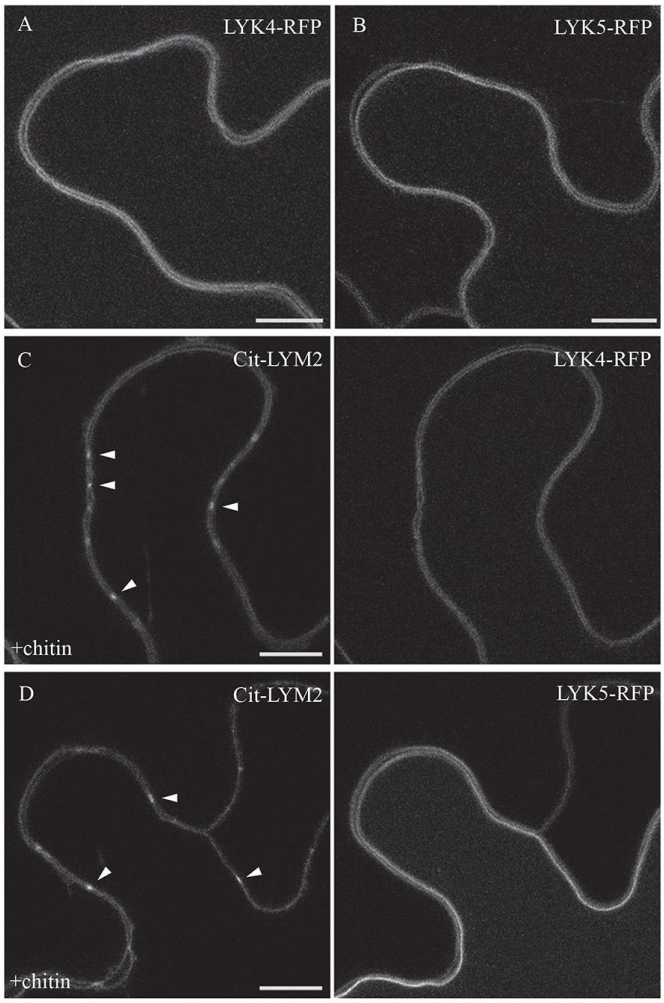

Figure S2

Figure S2. LYK4 and LYK5 localise to the PM. LYK4-RFP (A) and LYK5-RFP (B) localise evenly across plasma membrane when transiently expressed in *N.benthamiana*. (C) and (D) show localisation of LYK4-RFP and LYK5-RFP respectively in tissue that is co-expressing Citrine-LYM2 (Cit-LYM2) and has been treated with chitin for 30 min. Arrowheads identify Citrine-LYM2 marked plasmodesmata. Scale bars are 10 µm.

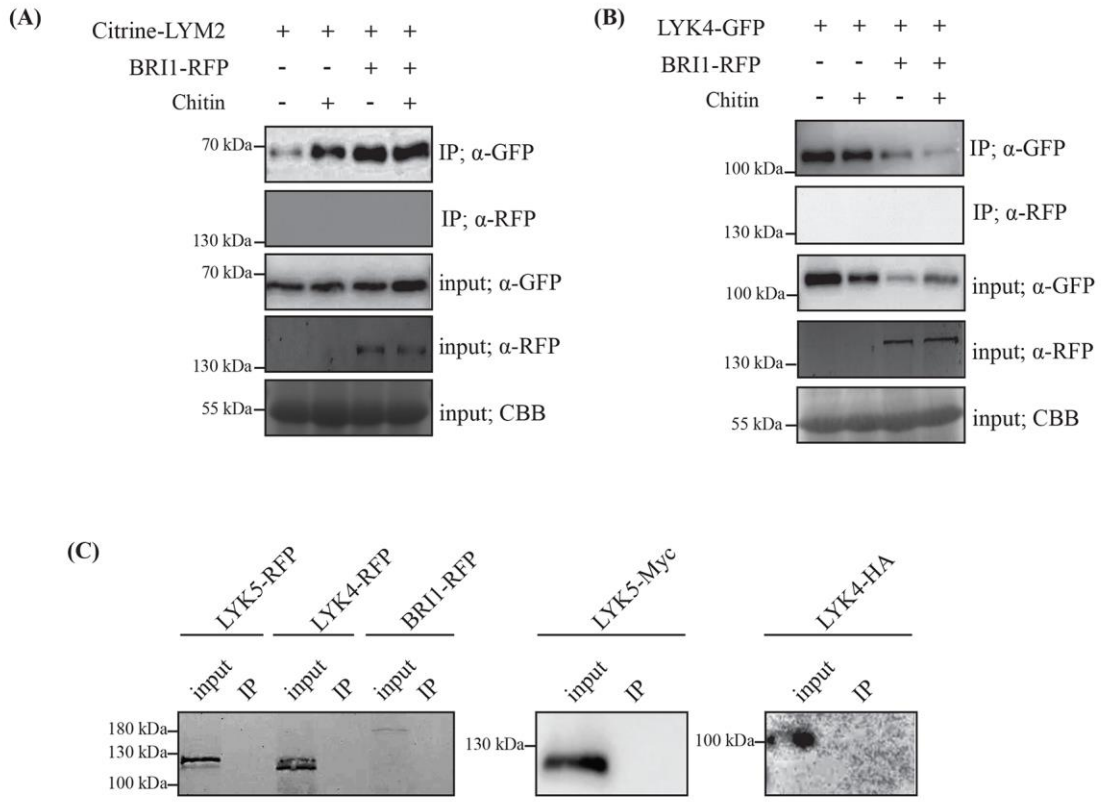

Figure S3

Figure S3. Negative controls for immunoprecipitation experiments. (A) and (B) Western blot analysis of immunoprecipitated protein extracts from *N. benthamiana* tissue expressing BRI1-RFP and either Citrine-LYM2 (A) or LYK4-GFP. (B) Citrine-LYM2 and LYK4-GFP were immunoprecipitated using GFP-trap beads and Western blots were probed with α-RFP to detect BRI1-RFP. Coomassie brilliant blue stained membranes serve as a loading control (CBB). Experiments were repeated three times with similar results. (C) LYK5-RFP, LYK4-RFP, BRI1-RFP, LYK5-Myc, LYK4-HA were immunoprecipitation with GFP-trap beads. Western blots of the input and immunoprecipitated (IP) samples were probed with antibodies α-RFP, α-Myc and α-HA.

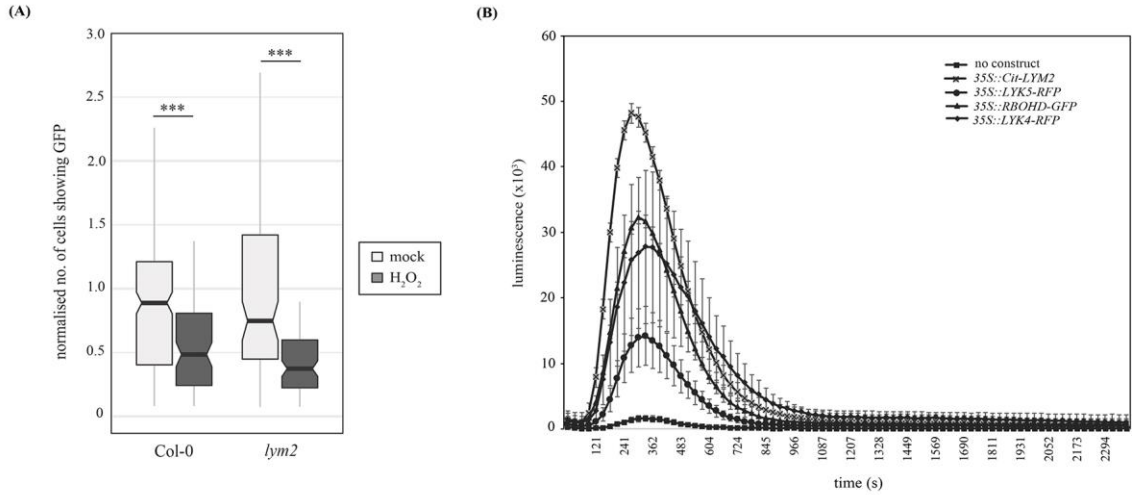

Figure S4

Figure S4. LYM2 acts upstream of ROS signalling in plasmodesmata closure

(A) Microprojectile bombardment into leaf tissue shows that H_2O_2 induces a reduction in GFP movement between cells in both Col-0 and *lym2-1* leaves. The number of cells showing GFP has been normalised to the mean of the mock data within genotypes. This data is summarised in box-plots in which the line within the box marks the median, the box signifies the upper and lower quartiles, the minimum and maximum within 1.5 × interquartile range. Data was analysed by a Students' t-test, or by a Mann-Whitney U-test for non-normal data ($n \geq 93$, ***p-value < 0.001). (B) Total accumulation of ROS in chitin-treated N. benthamiana leaf discs transiently expressing Citrine-LYM2, LYK4-RFP, LYK5-RFP, or RBOHD-GFP. Mean RLU are plotted over time (s). Error bars are SEM.

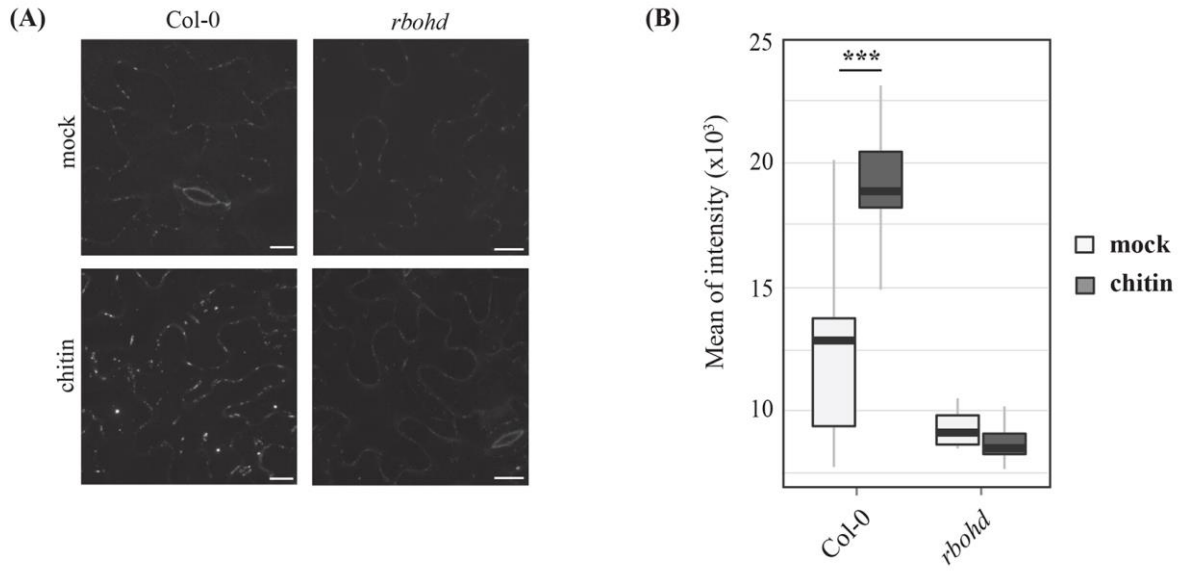

Figure S5

Figure S5. *rbohd* mutants do not deposit callose at plasmodesmata in response to chitin

(A) Confocal images of aniline blue stained plasmodesmal callose deposits in leaf tissue of 5–6-week-old leaves of Col-0 and *rbohd* mutant plants. Images were acquired 30 min post-infiltration with water or chitin. Scale bars are 15 µm. Images for Col-0 are as presented in Fig. 1B. (B) Quantification of plasmodesmata-associated fluorescence of aniline blue stained callose using automated image analysis. In contrast to Col-0, the *rbohd* mutant does not show increased aniline blue fluorescence at plasmodesmata in response to chitin. This correlates with the flux phenotype and identifies that chitin-triggered plasmodesmata closure is caused by callose deposition at plasmodesmata. The fluorescence intensity is summarised in box-plots in which the line within the box marks the median, the box signifies the upper and lower quartiles, the minimum and maximum within 1.5 × interquartile range. Data was analysed by pairwise Students' t-test comparing mock to chitin treated tissue within genotypes ($n \geq 31$, ***p-value < 0.001). Data for Col-0 is as presented in Fig. 1B.

1103 **Table S1.** n-values for experiments in which different samples had different numbers of
1104 replicates.

1105

Experiment	**n**	**Figure**
Bombardment		
col0-control	303	1A
col0-chitin	301	1A
lym2-control	101	1A
lym2-chitin	133	1A
lyk3-control	314	1A
lyk3-chitin	306	1A
lyk4-control	142	1A
lyk4-chitin	84	1A
lyk5-control	123	1A
lyk5-chitin	84	1A
rbohd-control	212	5A
rbohd-chitin	121	5A
bik1-control	93	5A
bik1-chitin	89	5A
S343A/S347A-control	114	5A
S343A/S347A-chitin	120	5A
S39A/S339A/S343A-control	111	5A
S39A/S339A/S343A-chitin	211	5A
S163A-control	225	5A
S163A-chitin	225	5A
S133A-control	227	5A
S133A-chitin	121	5A
cpk6-1-control	104	5A
cpk6-1-chitin	274	5A
cpk6-2-control	158	5A
cpk6-2-chitin	108	5A
col0-control	230	S4A

col0-H2O2	85	S4A
lym2-control	101	S4A
lym2-H2O2	91	S4A
Callose Staining		
col0-control	59	1B
col0-chitin	51	1B
lym2-control	40	1B
lym2-chitin	43	1B
lyk4-control	48	1B
lyk4-chitin	31	1B
lyk5-control	49	1B
lyk5-chitin	48	1B
cerk1-control	49	1B
cerk1-chitin	54	1B
rbohd-control	37	S5B
rbohd-chitin	45	S5B
PD Index		
control	31	4B
chitin	31	4B
Anisotropy		
GFP	11	4C
Cit-LYM2 PM	21	4C
Cit-LYM2 PD	21	4C
FRAP		
Cit-LYM2 chitin PD	43	4D
Cit-LYM2 chitin PM	45	4D
Cit-LYM2 water PD	46	4D
Cit-LYM2 water PM	52	4D
LYK4-RFP chitin PM	52	4D

LYK4-RFP water PM	60	4D
LYK5-RFP chitin PM	50	4D
LYK5-RFP water PM	50	4D
FLIM		
LYK4-GFP	110	3B
LYK4-GFP+LYK5-RFP	71	3B
LYK4-GFP+ BRI1-RFP	39	3B
LYK4-GFP+ CHITIN	29	3B
LYK4-GFP+ LYK5-RFP+ CHITIN	40	3B
LYK4-GFP+ BRI1-RFP+ CHITIN	19	3B
LYK4-GFP + Cit-LYM2 PM	44	3C
LYK4-GFP + LYK5-RFP + Cit-LYM2 PM	38	3C
LYK4-GFP + Cit-LYM2 PD	27	3C
LYK4-GFP + LYK5-RFP + Cit-LYM2 PD	33	3C

1106

1107